geodiversitas

2023 • 45 • 6

Stratigraphy of a middle Miocene neotropical Lagerstätte (La Venta Site, Colombia)

Laura MORA-ROJAS, Andrés CÁRDENAS, Carlos JARAMILLO, Daniele SILVESTRO, Germán BAYONA, Sebastián ZAPATA, Federico MORENO, César SILVA, Jorge MORENO-BERNAL, Juan Sebastián JARAMILLO, Victor VALENCIA & Mauricio IBAÑEZ

in Juan D. CARRILLO (ed.),
Neotropical palaeontology: the Miocene La Venta biome

art. 45 (6) — Published on 13 April 2023
www.geodiversitas.com

PUBLICATIONS SCIENTIFIQUES

MUSÉUM NAL HIST NATURELLE

Geodiversitas est indexé dans / Geodiversitas *is indexed in:*
– Science Citation Index Expanded (SciSearch®)
– ISI Alerting Services®
– Current Contents® / Physical, Chemical, and Earth Sciences®
– Scopus®

Geodiversitas est distribué en version électronique par / Geodiversitas *is distributed electronically by:*
– BioOne® (http://www.bioone.org)

Les articles ainsi que les nouveautés nomenclaturales publiés dans *Geodiversitas* sont référencés par / *Articles and nomenclatural novelties published in* Geodiversitas *are referenced by:*
– ZooBank® (http://zoobank.org)

Geodiversitas est une revue en flux continu publiée par les Publications scientifiques du Muséum, Paris
Geodiversitas *is a fast track journal published by the Museum Science Press, Paris*

Les Publications scientifiques du Muséum publient aussi / *The Museum Science Press also publish:* ***Adansonia***, ***Zoosystema***, ***Anthropozoologica***, ***European Journal of Taxonomy***, ***Naturae***, ***Cryptogamie*** **sous-sections** ***Algologie***, ***Bryologie***, ***Mycologie, Comptes Rendus Palevol***

Diffusion – Publications scientifiques Muséum national d'Histoire naturelle
CP 41 – 57 rue Cuvier F-75231 Paris cedex 05 (France)
Tél. : 33 (0)1 40 79 48 05 / Fax : 33 (0)1 40 79 38 40
diff.pub@mnhn.fr / http://sciencepress.mnhn.fr

ISSN (imprimé / *print*) : 1280-9659/ ISSN (électronique / *electronic*) : 1638-9395

Stratigraphy of a middle Miocene neotropical Lagerstätte (La Venta Site, Colombia)

Laura MORA-ROJAS
Andrés CÁRDENAS
Escuela de Ciencias Aplicadas e Ingeniería, Universidad EAFIT,
Carrera 49 # 7 sur – 50, Medellín (Colombia)
lmorar@eafit.edu.co
acarde17@eafit.edu.co (corresponding autor)

Carlos JARAMILLO
Smithsonian Tropical Research Insitute, Edificio 401,
Tupper, Balboa, Panama city (Panama)
jaramilloc@si.edu

Daniele SILVESTRO
Department of Biology, University of Fribourg,
Chemin du Musée 10, 1700 Fribourg (Switzerland)
and Department of Biological and Environmental Sciences,
University of Gothenburg, Gothenburg, Sweden Carl Skottsbergs gata 22B,
Gothenburg 413 19, Sweden Gothenburg Global Biodiversity Centre (Sweden)
daniele.silvestro@unifr.ch

Germán BAYONA
Corporación Geológica ARES, Calle 26 # 69C-03,
Torre C, Oficina 904, Bogotá (Colombia)
gbayona@cgares.org

Sebastián ZAPATA
Facultad de Ciencias Naturales, Universidad del Rosario,
Calle 12C # 6-25, Bogotá (Colombia)
and Smithsonian Tropical Research Insitute, Edificio 401,
Tupper, Balboa, Panama city (Panama)
szapatah@gmail.com

Federico MORENO
Department of Geosciences, University of Arizona,
1040 E. 4th Street, Tucson, AZ 85721 (United States)
federicomrn@email.arizona.edu

César SILVA
Smithsonian Tropical Research Insitute, Edificio 401,
Tupper, Balboa, Panama city (Panama)
casilvacar@yahoo.es

Jorge W. MORENO-BERNAL
Departamento de Física y Geociencias, Universidad del Norte,
km 5 vía Puerto Colombia, Barranquilla (Colombia)
jwmoreno@uninorte.edu.co

Juan Sebastián JARAMILLO
Escuela de Geociencias, Universidad Nacional de Colombia,
Calle 59A # 63-20, Medellín (Colombia)
jusjaramillori@unal.edu.co

Victor VALENCIA
School of the Environment, Washington State University,
Pullman, WA 99163(United States)
victor.valencia@wsu.edu

Mauricio IBAÑEZ
Department of Geosciences, University of Arizona,
1040 E. 4th Street, Tucson, AZ 85721 (United States)
ibanezm@arizona.edu

Submitted on 22 April 2022 | accepted on 12 September 2022 | published on 13 April 2023

urn:lsid:zoobank.org:pub:AD31694E-DD43-495D-BBD3-549B463AF2D3

Mora-Rojas L., Cárdenas A., Jaramillo C., Silvestro D., Bayona G., Zapata S., Moreno F., Silva C., Moreno-Bernal J. W., Jaramillo J. S., Valencia V. & Ibañez M. 2023. — Stratigraphy of a middle Miocene neotropical Lagerstätte (La Venta Site, Colombia), *in* Carrillo J. D. (ed.), Neotropical palaeontology: the Miocene La Venta biome. *Geodiversitas* 45 (6): 197-221. https://doi.org/10.5252/geodiversitas2023v45a6. http://geodiversitas.com/45/6

ABSTRACT
The middle Miocene Konzentrat-Lagerstätte of the La Venta site recorded in the Honda Group contains invaluable information on the biotic response to the climatic changes of the Miocene Climatic Transition. Its fossil record has been studied for almost a century and offers one of the best windows to the Neotropics terrestrial ecosystems during the Neogene. We have compiled all published studies and, using graphic correlation and a recently published geological map for the region, placed them into a composite standard section. Furthermore, we improved its chronostratigraphic control by analyzing new geochronological data (U-Pb in zircons) and developing a probabilistic age model using a Bayesian framework. The results suggest that most of the fossil assemblage of the Honda Group accumulated in a meandriform fluvial system (upper part of La Victoria Formation – lower part of Villavieja Formation) that later shifted to an anastomosed system (upper part of Villavieja Formation). The *c.* 552-m-thick La Victoria Formation is younger than 16 Ma and older than 12.58 Ma, whereas the *c.* 569-m-thick Villavieja Formation is younger than 12.58 Ma and older than 10.52 Ma. The La Venta site is crucial for understanding Miocene paleoecological dynamics in northern South America, but despite decades of studies, it is still in the early phase of exploration.

KEY WORDS
Depositional systems, geochronology, Honda Group, probabilistic age model, sedimentation rates.

RÉSUMÉ
Stratigraphie d'un Lagerstätte néotropical du Miocène moyen (site de La Venta, Colombie).
Le Konzentrat-Lagerstätte du Miocène moyen du site de La Venta, situé dans le Groupe Honda, en Colombie, contient des informations inestimables sur la réponse biotique tropicale aux changements de la transition climatique du Miocène. Son registre fossile, étudié pendant près d'un siècle, offre l'une des meilleures fenêtres sur les écosystèmes terrestres néotropicaux au cours du Néogène. Nous avons compilé ici toutes les études publiées, puis nous les avons replacées dans une coupe synthétique standard, résultant de corrélations stratigraphiques et d'une carte géologique récente. De plus, nous avons amélioré son contrôle chronostratigraphique en analysant de nouvelles données géochronologiques (U-Pb dans les zircons) et en développant un modèle d'âge probabiliste utilisant une méthode bayésienne. Les résultats suggèrent que la plupart des assemblages fossiles du Groupe Honda se sont accumulés dans un système fluvial méandriforme (partie supérieure de la Formation de La Victoria – partie inférieure de la Formation de Villavieja) qui s'est ensuite déplacé vers un système anastomosé (partie supérieure de la Formation de Villavieja). La Formation de La Victoria, d'une épaisseur de 552 m, est plus récente que 16 Ma et plus ancienne que 12,58 Ma, tandis que la Formation de Villavieja, d'une épaisseur de 569 m, est plus récente que 12,58 Ma et et plus ancienne que 10,52 Ma. Le site de La Venta est fondamental pour comprendre la dynamique paléoécologique du Miocène dans le nord de l'Amérique du Sud mais malgré des décennies d'études, il en est encore dans sa phase initiale d'exploration.

MOTS CLÉS
Systèmes de dépôt, géochronologie, Groupe Honda, modèle d'âge probaliste, taux de sedimentation.

RESUMEN

Estratigrafía de un Lagerstätte neotropical del Mioceno medio (localidad de La Venta, Colombia).

El Konzentrat-Lagerstätte del Mioceno medio de la localidad de La Venta registrado en el Grupo Honda contiene información invaluable sobre la respuesta biótica a los cambios climáticos de la Transición Climática del Mioceno. Su registro fósil ha sido estudiado durante casi un siglo y ofrece una de las mejores ventanas a los ecosistemas terrestres del Neotrópico durante el Neógeno. Hemos compilado todos los estudios publicados y, utilizando la correlación gráfica y un mapa geológico recientemente publicado para la región, los pusimos en un solo marco estratigráfico. Además, mejoramos su control cronoestratigráfico analizando nuevos datos geocronológicos (U-Pb en circones) y desarrollamos un modelo de edad probabilístico utilizando un método Bayesiano. Los resultados sugieren que la mayor parte de la asociación fósil del Grupo Honda se acumuló en un sistema fluvial meandriforme (parte superior de la Formación La Victoria – parte inferior de la Formación Villavieja) que luego se transformó en un sistema anastomosado (parte superior de la Formación Villavieja). La Formación La Victoria de *c.* 552 m de espesor es menor a 16 Ma y mayor a 12.58 Ma, mientras que la Formación Villavieja de *c.* 569 m de espesor es menor a 12.58 Ma y mayor a 10.52 Ma. La localidad de La Venta es crucial para comprender las dinámicas paleoecológicas del Mioceno en el norte de América del Sur, pero a pesar de décadas de estudios, todavía se encuentra en la fase inicial de exploración.

PALABRAS CLAVE
Sistemas de acumulación, geocronología, Grupo Honda, modelo probabilístico de edad, tasas de sedimentación.

INTRODUCTION

La Venta is a middle Miocene Konzentrat-Lagerstätte accumulated in the sedimentary succession of the Honda Group in the Upper Magdalena Valley, Colombia (Fig. 1). It is one of the most studied Neogene Neotropical vertebrate faunal fossil assemblages (e.g., Kay & Madden 1997a, b; Madden *et al.* 1997a, b; Carrillo *et al.* 2015) with 166 (91.3%) publications focusing on taxonomy and systematics, 11 (6%) on paleoecology, and 5 (2.7%) on paleobiogeography (Supplementary Information, Appendix 1). The Honda Group accumulated at La Venta mostly during a *c.* 2-million-year span of the middle to late Miocene (*c.* 13.5 to *c.* 11.5 Ma, Guerrero 1993, 1997; Flynn *et al.* 1997) and therefore is an ideal setting for examining tropical ecosystems during the middle Miocene Climatic Transition – a time interval with a decrease in both CO_2 levels and global temperatures (Flower & Kennett 1994; Zachos *et al.* 2001, 2008) together with the tectonic effects associated with the rise of the Central and Eastern Cordilleras of Colombia (Guerrero 1997; Anderson *et al.* 2016; Montes *et al.* 2021).

Research at La Venta region is still in its early phase, and large unexplored areas are likely to yield an abundant fossil record. Furthermore, paleobiological and paleoecological studies may be able to help us track the fate of individual clades along the timespan that is exposed at La Venta and to understand the ecosystem as a whole. These detailed studies require a precise stratigraphical location of all fossil-bearing horizons and refined age determinations. We present a composite standard section of the Honda Group, which includes eleven detailed sections (i.e., bed resolution) that are pieced together using Guerrero's (1997) stratigraphic framework. We also provide a paleoenvironmental interpretation of the sedimentary succession, report four new U/Pb geochronological dates and use a Bayesian analysis to build an age model for the entire sequence. We placed all the beds with fossil occurrences, taken from all published studies of La Venta, on the most updated geological map (Montes *et al.* 2021). The stratigraphic framework presented here facilitates the integration of past with future studies, allowing a better stratigraphic control of the many studies that will continue being produced at La Venta.

STRATIGRAPHIC BACKGROUND

Hettner (1892) introduced the name "Hondasandstein" referring to the tufa-like greenish-grey sandstone of the "Tertiary?" age that outcrops on both banks of the Magdalena River near Honda, Tolima. Royo y Gómez (1941, 1942) informally defined the Honda Formation and identified two stratigraphic units based on the occurrence of andesite cobbles (absent in the lower unit while present in the upper unit). Butler (1942) defined formally the Honda Series, using as the type locality the "Cordillera de San Antonio" and expanded the lower boundary to include some red layers. Stirton (1953a, b) raised the Honda Formation rank to Group, and since then several authors, including Fields (1959); Wellman (1970), Takai & Setoguchi (1990); Takai *et al.* (1992); Villarroel *et al.* (1996); and Guerrero (1997) have established different stratigraphic nomenclatures for the sequence outcropping in La Venta (Table 1).

TECTONIC EVOLUTION OF THE UPPER MAGDALENA BASIN

The Upper Magdalena Valley (UMV) basin is located between the Central and Eastern Colombian Cordilleras. After a non-depositional and deformation interval from Middle Jurassic to Barremian (gap of *c.* 35-40 Ma), an Aptian extensional tectonism allowed the onset of continental to marginal deposi-

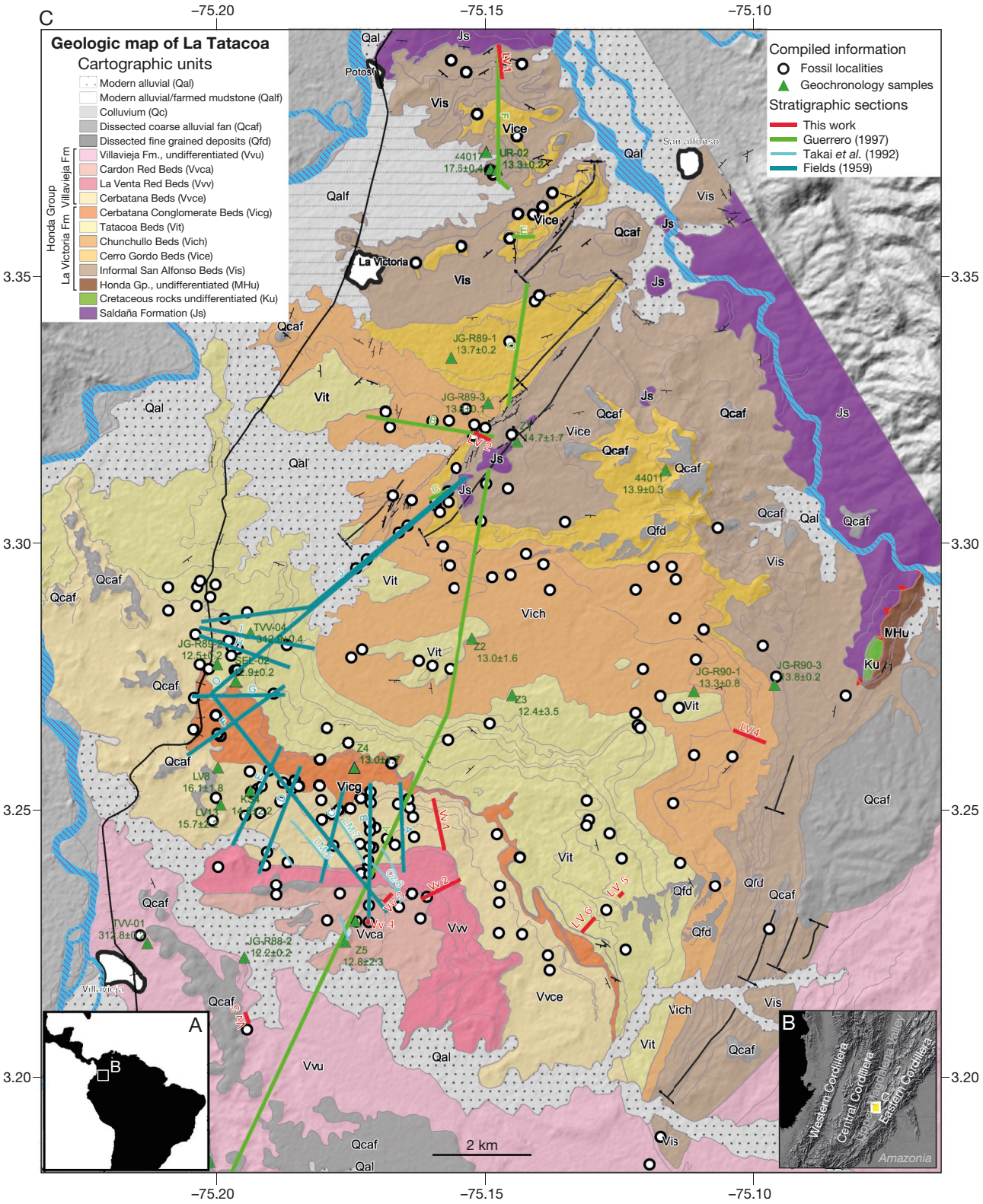

FIG. 1. — Fossil localities, stratigraphic sections, and geochronology samples placed in the geologic map of Montes *et al.* (2021): **A**, location of La Venta Site in South America; **B**, location of La Venta Site in the northern Andes; **C**, geologic map of La Venta Site (Montes *et al.* 2021).

tion that rests in angular unconformity with Middle Jurassic volcanic rocks of the Saldaña Formation (Rodríguez *et al.* 2018), and changes up-section to shallow-marine deposition in Albian to mid-Campanian time (Ramón & Rosero 2006; Sarmiento-Rojas *et al.* 2006; Borrero *et al.* 2012; Zapata *et al.* 2019; Valencia-Gómez *et al.* 2020). Late Campanian

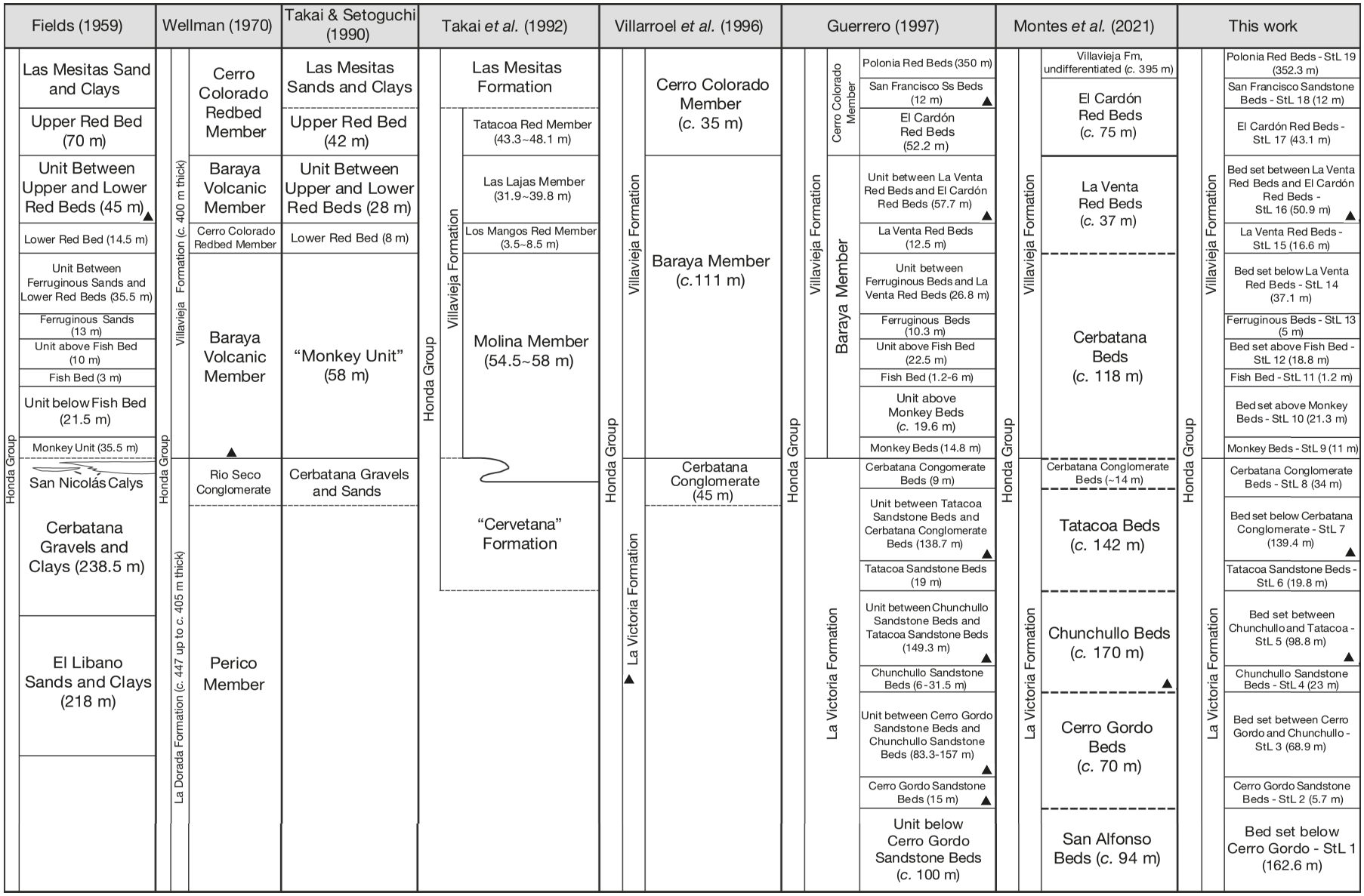

TABLE 1. — Historical lithostratigraphic framework for the Honda Group at La Venta site. **StL**, Stratigraphic level. ▲, Volcanoclastic.

to Paleogene strata record syn-orogenic sedimentation associated with the deformation of the present Central Cordillera and internal segments of the Magdalena Valley (e.g., Pacande high; Anderson *et al.* 2016; Sarmiento & Rangel 2004; Bayona 2018; Horton *et al.* 2020). The rise of the southern segment of the Eastern Cordillera during the late Miocene (*c.* 10 Ma) fragmented the basin and produced the onset of intermountain basin sedimentation (Anderson *et al.* 2016). Sedimentary and volcanoclastic strata deposited in the UMV during the middle Miocene were sourced mainly from exposed rocks in the Central Cordillera (Van Houten & Travis 1968; Anderson *et al.* 2016) and the active volcanic activity from the Cauca-Patia magmatic center (Montes *et al.* 2021). Guerrero (1997) and Anderson *et al.* (2016) suggested that disconnected basement highs from the Eastern Cordillera were also source area during the late Miocene, but there was not a continuous orographic barrier separating the UMV from Amazonia until the late Miocene-Pliocene (Fig. 1B) (Anderson *et al.* 2016; Montes *et al.* 2021).

THE MIDDLE MIOCENE CLIMATE

The global climate during the middle Miocene is characterized by two phases, the middle Miocene Climate Optimum [MMCO; *c.* 17-14.7 Ma; Holbourn *et al.* (2015)] and the middle Miocene Climatic Transition [MMCT; *c.* 14.2-13.8 Ma; Hamon *et al.* (2013)]. During the MMCO, global temperatures increased reaching a peak *c.* 16 Ma (Zachos *et al.* 2001, 2008); atmospheric CO2 levels rose to 460-600 ppm (Zachos *et al.* 2001, 2008; Steinthorsdottir *et al.* 2021), bottom-water temperatures were 5-9°C warmer than today (Steinthorsdottir *et al.* 2021), global mean annual surface temperature reached *c.* 18.4°C (You *et al.* 2009), and tropical sea-surface temperatures were 3-4°C warmer than today (Steinthorsdottir *et al.* 2021). During the MMCT and the remainder of the middle and late Miocene, both global temperatures and CO_2 decreased (Steinthorsdottir *et al.* 2021) and the formation of the East Antarctic Ice Sheet accelerated (Flower & Kennett 1994).

METHODS

Lithostratigraphy

We measured and described eleven stratigraphic sections at 1:500 scale using the Jacob staff, tape measure, compass, and linear traverses. Five of these stratigraphic sections are in the La Victoria Formation (from base to top: LV 1, LV 2, LV 4, LV 5, and LV 6) and six in the Villavieja Formation (from base to top: Vv 1, Vv 2, Vv 3, Vv 4, Vv 5, and Vv 6) (Figs 1; 2). Additionally, using the SDAR package (Ortiz & Jaramillo 2020), we recorded the stratigraphic information for all the stratigraphic columns (Supplementary material, Appendices 2, 3, and 4).

To build a composite standard section (CS) of the La Venta area (Fig. 2) first we located all the stratigraphic sections measured in previous studies and in this study on the geologic map of Montes *et al.* (2021) (Fig. 1). Then, we made a lithostratigraphic correlation between the sections measured in this study and the sections A and B from Guerrero (1997). Correlations were made by using: Guerrero's (1997) StLs (i.e. 1, 2, 3, 4, 5, 7, 8, 9, 10, 11, 12, 13, 14, 15, 16, 17, and 19), the tops of the cartographic geological units of Montes *et al.* (2021) as reliable correlation horizons in continental fluvial systems (taking into account lateral accretion sets at local scale that indicate lateral change of lithofacies), and key fossil assemblages among the sections applying the graphic correlation method (Shaw 1964). Moreover, we calculated the stratigraphic thickness of intervals defined in the CS using the equation ST = Sen α × L, where ST is the stratigraphic thickness, α is the dip angle of the closest structural datapoint, and L is the longitude of the section in the map. Alphas were taken from Guerrero's (1997) and Montes' *et al.* (2021) maps. Therefore, this CS covers the entire stratigraphic sequence outcropping in La Venta and contains our eleven sections and sections A and B of Guerrero (1997) (Fig. 2; extended lithological resolution at Supplementary material Appendix 6). The description includes bed-by-bed lithofacies following the criteria of Allen (1982), Reineck & Singh (1986), Einsele (2000), and Miall (2006), which include rock type, grain size, matrix content, physical sedimentary structures, bioturbation, color, gradation, fossils, and other allochemical particles (Supplementary material, Appendices 6; 7). We used these lithofacies and Walther's Law (Middleton 1973) to determine lithofacies associations and interpret depositional environments (Fig. 2; Tables 2, 3; and Supplementary material, Appendices 6; 7).

Geochronology

New zircon geochronology samples were collected in the Villavieja and the La Victoria formations to complement the available geochronological data and thus improve the precision of our age model. We dated four samples using U-Pb detrital zircon (44017, Lat. 3.3733, Long. –75.1497 [3°22'23"N, 75°8'58"W], stratigraphic meter 63.5; 44011, Lat. 3.3137, Long. –75.1164 [3°18'49"N, 75°6'59"W], stratigraphic meter 218.8; TVV-04, Lat. 3.2831, Long. –75.1937 [3°16'59"N, 75°11'37"W], stratigraphic meter 474; and TVV-01, Lat. 3.2251, Long. –75.2129 [3°13'30"N, 75°12'46"W], stratigraphic meter 932). Samples 44017, 44011, and TVV-04 corresponded to a tuffaceous sandstone and were collected to increase the possibility of having syn-sedimentary volcanic zircons, while sample TVV-01 was collected to improve the geochronological record towards the top of the stratigraphic section. Zircon grains were concentrated by using standard techniques, including mechanical crushing, pulverization, magnetic separation, and heavy liquids (methylene iodide, 3.30-3.33 g/cm^3) following the Zirchron® method. Samples 44017 and 44011 were analyzed at the University of Arizona Laserchron Center. U-Pb single grain zircon geochronology was conducted by using a multicollector inductively coupled plasma-mass spectrometer coupled to a 193 nm Excimer laser ablation system following the method presented in Gehrels *et al.*

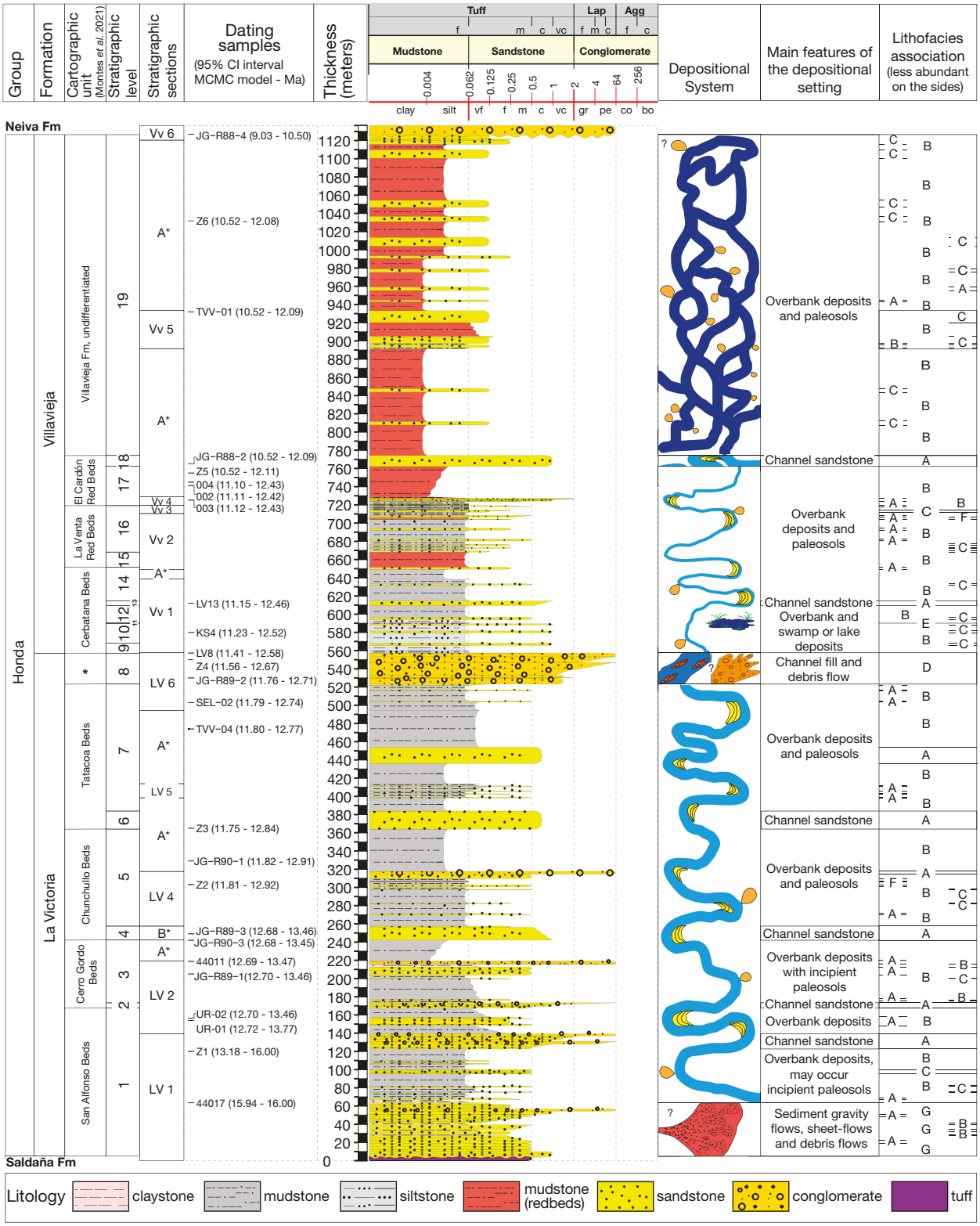

FIG. 2. — Composite standard section (**CS**) of the Honda Group at the La Venta site. We estimated the stratigraphic position of geochronology samples from information reported in the literature, graphic correlations (Supplementary material, Appendix 5), and the geologic map of Montes *et al.* (2021). Depositional systems, main features of the depositional settings, and lithofacies associations are on the right side of the CS. Cartographic unit: *, Cerbatana Conglomerate Beds; Stratigraphic levels: **, 11 (Fish Bed); ***, 13 (Ferruginous Beds). Stratigraphic sections: **LV1**, **LV2**, **LV4**, **LV5**, **LV6**, **Vv1**, **Vv2**, **Vv3**, **Vv4**, **Vv5**, **Vv6**, this work. Stratigraphic sections: **A***, **B***, Guerrero 1997. Geochronology sample references: Takemura *et al.* (1992): 002, 003, and 004; Takemura & Danhara (1985): LV8, KS4 and LV13; Flynn *et al.* (1997): JG-R89-2, JG-R89-3, and JG-R88-2; Anderson *et al.* (2016): Z1, Z2, Z3, Z4, and Z5; Cadena *et al.* (2020): 46311(UR-01) and 46312 (UR-02); Montes *et al.* (2021): SEL-02; this work: 44017, 44011, TVV-04, and TVV-01. The stratigraphic position of geochronology samples was estimated by authors' reported information, graphic correlations, and the cartography of Montes *et al.* (2021).

TABLE 2. — Equivalence between the facies scheme proposed by Miall (2006) and the detailed lithofacies defined in the composite standard section. Symbol: *, modified for a comprehensive description.

Basic facies code (*sensu* Miall 2006)	Facies (*sensu* Miall 2006)	Sedimentary structures (*sensu* Miall 2006)	Interpretation (*sensu* Miall 2006)	Equivalence with detailed lithofacies (this work)	Meaning detailed lithofacies	Interpretation detailed lithofacies (this work)
Gmg	Matrix-supported gravel	Inverse to normal grading	Pseudoplastic debris flow (low strength, viscous)	(c)S-Cms_iG	Conglomeratic sandstone to matrix supported conglomerate with inverse gradation	Flow with high transport and deposit capacity, with signs of substrate erosion and evidence of soil formation processes
Gh	Clast-supported crudely bedded gravel	-	Longitudinal bed forms	C_dBc	Conglomerate with diffuse bed contacts which lack well-defined stratification	Longitudinal bed forms result of secondary flows (non-cohesive), lag deposit
Sl-Gt	Pebbly sand to gravel, stratified	Low-angle (<15°) cross-beds - trough cross-beds	Scour fills, humpback or washed-out dunes, antidunes and trough cross-beds	(c)S_Cms_Epsi_w-s	Conglomeratic sandstone to matrix supported conglomerate with epsilon stratification and wedge-shaped structures	Conglomeratic sand to conglomerate bars with lateral accretion evidence
Gp	Gravel, stratified	Planar cross-beds	Transverse bedforms, deltaic growths from older bar remains	C_Xp	Conglomerate with planar cross-stratification	Conglomerate transverse bars
Sm-Gmm*	Sand, fine to coarse - Matrix-supported gravel*	Massive or faint lamination-Weak grading	Sediment-gravity flow deposits - Pseudo-plastic debris flow (high-strength, viscous)	(c)S-Cms_ma_Clens	Conglomeratic sandstone to matrix supported conglomerate, massive and conglomeratic lenses	Flow with high transport and deposit capacity / Debris flow (viscous and with high concentration of sediments)
St	Sand fine to very coarse, may be pebbly	Solitary or grouped trough cross-beds - Broad shallow scours	Sinuous-crested and linguoid (3-D) dunes - Scour fill	(c)S_Clens_w-s_Xt	Conglomeratic sandstone (fine to coarse-grained), with conglomeratic lenses, wedge-shaped structures and trough cross-bedding	Sand bar migration in channel floor
Sp	Sand fine to very coarse, may be pebbly	Solitary or grouped planar cross-beds	Transverse and linguoid bedforms (2-D dunes)	(m)S(m)_Xp	Muddy sandstone, medium-grained and cross stratification (planar)	Sediment accumulation on bars of channel floor by very low energy currents
Sh-St*	Sand fine to coarse, may be pebbly	Horizontal lamination parting or streaming lineation	Plane-bed flow (critical flow) - Sinuous-crested and linguoid (3-D) dunes	S(m)_Ppl_Xt_Clen_Intra	Sand medium-grained, with planar parallel lamination (at the base), planar cross-bedding (at the top), with conglomeratic lenses and intraclasts	Sand bar / Upper flow regime - decreasing in the flow regime
Sp-St	Sand fine to very coarse, may be pebbly	Solitary or grouped planar cross-beds	Transverse and linguoid bedforms (2-D dunes) - Sinuous-crested and linguoid (3-D) dunes	S(f-c)_Xpt (c)S_Xpt	Sandstone (fine to coarse grain sized, occasionally very coarse) with cross-stratification (planar or through) Conglomeratic sandstone with cross-stratification (planar or trough). Both may have conglomeratic lenses	Sand bar migration in channel floor Sand bar migration in channel floor
Sr-Fm*	Sand, very fine – Silt, mud	Massive*	Sand with dewatering or bioturbation* – Overbank, abandoned channel or drape deposits	(m)S_ma_Red-mot_uG	Muddy sandstone (very fine-grained), massive, Red, mottled and ungraded	Sediments accumulated by hyperconcentrated flows with subaerial exposure
Sr	Sand very fine to coarse	Ripple cross-lamination	Ripples (lower flow regime)	S(m-c)_uCr_uG	Sandstone (medium to coarse grained) with undulate current ripples and ungraded	Sand accumulated by flows with low velocities (lower flow regime) / undulate currents

(2006, 2008). TVV-04, and TVV-01, were analyzed at the Radiogenic Isotope and Geochronology Lab (RIGL) at Washington State University. The analyses were done with a Teledyne Analyte Excite 193 nm excimer laser ablation system coupled to a Thermo Finnigan Element2 ICPMS following the protocol proposed by Chang *et al.* (2006). The lead isotopic ratios were corrected for common Pb, using the measured 204Pb, assuming an initial Pb composition according to Stacey & Kramers (1975) and respective uncertainties of 1.0, 0.3, and 2.0 for 206Pb/204Pb, 207Pb/204Pb, and 208Pb/204Pb. The age of standard, the calibration correction from standard, the composition of the common Pb, and the constant decay uncertainty are grouped and are known as the systematic error.

The results of our four samples were combined with the published geochronology that includes fission tracks in zircon ages (samples LV8, KS4, LV13, 002, 003, and 004; Takemura & Danhara 1985; Takemura *et al.* 1992), Ar/Ar ages on detrital plagioclase and hornblende (samples JG-R89-2, JG-R90-1, JG-R90-3, JG-R89-1, JG-R89-3, JG-R88-4; Flynn *et al.* 1997), and U-Pb detrital zircon ages (samples Z1, Z2, Z3, Z4, Z5, Z6, UR-01, UR-02, and

Table 2. — Continuation.

Basic facies code (*sensu* Miall 2006)	Facies (*sensu* Miall 2006)	Sedimentary structures (*sensu* Miall 2006)	Interpretation (*sensu* Miall 2006)	Equivalence with detailed lithofacies (this work)	Meaning detailed lithofacies	Interpretation detailed lithofacies (this work)
Sh*	Sand very fine to coarse, may be pebbly	Horizontal lamination parting or streaming lineation	Plane-bed flow (critical flow)/or lower flow velocities during the initial movement of a sand bed	S_Ppl_uG_ CaNod	Sandstone with planar parallel lamination, ungraded and calcareous nodules	Sand bars in channel floor or high energy currents
				(m)S(f-m)_Ppl	Muddy sandstone, fine to medium-grained and planar parallel lamination	Suspension-load deposits in the flood plain
				S(f)_nG	Sandstone with fine grain-sized and normal gradation	Sand bars in channel floor / current flows with energy decreasing
				S(f-vc)_Ppl	Very fine to coarse grained sandstone with planar parallel lamination. May include intraclasts.	Upper flow regime / or sand bars in the channel floor
Sl	Sand, fine to coarse, may pebbly	Low-angle (<15°) cross-beds	Scour fills, humpback or washed-out dunes, antidunes	(c)S_S_ Epsi_w-s	Conglomeratic sandstone /or sandstone with epsilon stratification and/or wedge-shaped structures	Bar deposits (with lateral accretion) in the channel floor
Sm	Sand, fine to coarse	Massive, or faint lamination	Sediment gravity-flow deposits	S_ma_iG	Massive muddy sandstone inverse grading	Deposits of sediment gravity-flow / hyperconcentrated flows
				S_ma_uG	Massive sandstone ungraded	Deposits of sediment gravity-flow / hyperconcentrated flows
				(m)S_ma_uG	Massive muddy sandstone ungraded which may include calcareous nodules	Deposits of sediment gravity-flow / hyperconcentrated flows
				S_ma_uG_ CaNod	Massive sandstone (it may be muddy) ungraded, with calcareous nodules	Deposits of sediment gravity-flow / hyperconcentrated flow affected by soil formation processes
Sh-Fl*	Sand fine	Horizontal lamination parting - Fine lamination	Lower flow velocities - Overbank, abandoned channel or waning flood deposits	(m)S_(Car) Fc-s_Ppl	Muddy sandstone fine-grained gray color, with carbonaceous mudstone sheets and planar parallel lamination	Lower flow velocity, with intermittent supply of organic matter with signs of conditions related to reducing environments
Fl	Sand, silt mud	Fine lamination, very small ripples	Overbank, abandoned channel, or waning flood deposits	Fc-s_Ppl	Mudstone with planar parallel lamination, it may have normal gradation	Sediments accumulation by suspension in flood plains
Fl	Sand, silt mud	Fine lamination, very small ripples	Overbank, abandoned channel, or waning flood deposits	(s)Fc-s_nG	Mudstone with normal gradation from very fine sand to mudstone	Sediments accumulation by suspension in flood plains affected by currents with energy changes
				Fc-s_Ppl_nG	Mudstone with planar parallel lamination and normal gradation	Sediments accumulation by suspension in flood plains affected by currents with energy changes
				(s)Fc-s_Ppl_ nG	Sandy mudstone with planar parallel lamination and normal gradation	Sediments accumulation by suspension in flood plains affected by currents with energy changes
				Fc-s_CaNod	Mudstone with calcareous/ or ferruginous nodules	Sediments accumulation by suspension in flood plains / affected by soil formation processes
				Fc-s_Ppl_var	Varicolored mudstone with planar parallel lamination	Sediments accumulation by suspension in flood plains affected by soil formation processes
				(s)Fc-s_Ppl_ var	Sandy mudstone with planar parallel lamination and varicolored	Sediments accumulation by suspension in flood plains / affected by soil formation processes
				(s)Fc-s_Ppl_ nG_var	Sandy mudstone with planar parallel lamination, normal gradation (from light green sandy mudstone to varicolored red claystone)	Sediments accumulation by suspension in flood plains, affected by variations in the water table, which produces developed of soil horizons

SEL-02; Montes *et al.* 2021; Anderson *et al.* 2016; Cadena *et al.* 2020; Figs 3; 4). We located all the geochronological samples in our CS using the information provided by each author and the map of Montes *et al.* (2021) (for additional details, see Supplementary materials Appendix 10). The Maximum Depositional Age (MDA) of each individual sample was determined by excluding zircon grains with percentage errors higher than 20% and calculating the mean average of the three youngest populations (which are overlapping in age at 2 SD; Dickinson & Gehrels 2009) and a Mean Square Weighted Deviation < 1, which is a statistically reliable MDA calculation (Coutts *et al.* 2019; Herriott *et al.* 2019). Since zircon grains from the youngest age population are not necessarily cogenetic, we also present the youngest zircon age (Coutts *et al.* 2019). Age populations and age peaks were extracted from the age distribution using a probability density plot (Ludwig 2012; Supplementary material Appendix 8).

Table 2. — Continuation.

Basic facies code (*sensu* Miall 2006)	Facies (*sensu* Miall 2006)	Sedimentary structures (*sensu* Miall 2006)	Interpretation (*sensu* Miall 2006)	Equivalence with detailed lithofacies (this work)	Meaning detailed lithofacies	Interpretation detailed lithofacies (this work)
Fsm	Sil, mud	Massive	Backswamp or abandoned channel, or drape deposits	Fc-s_ma_Fish	Massive green mudstone, very fossiliferous with abundant fish remains, coprolites, and another vertebrate remains	Sediment accumulation by suspension in a reducing environment / back swamp or oxbow lake
Fm	Mud, silt	Massive, desiccation cracks	Overbank, abandoned channel, or drape deposits	Fc-s_ma_Red	Mudstone, massive and red-colored	Sediments accumulation by suspension in flood plains whit subaerial exposure
				(s)Fc-s_ma	Massive sandy mudstone	Sediments accumulation by suspension in flood plains
				Fc-s_ma	Massive mudstone	Sediments accumulation by suspension in flood plains
				Fc-s_Ppl_Red	Red mudstone with planar parallel lamination	Sediments accumulation by suspension in flood plains whit subaerial exposure
Fr	Mud, silt	Massive, roots, bioturbation	Root bed, incipient soil	(s)Fc-s_ma_ Red-mot	Sandy mudstone massive and mottled, red colored	Sediments accumulated by suspension with subaerial exposition - soil formation processes in flood plains
				Fc-s_ma_Red-var	Mudstone massive Red varicolored	Sediments accumulated by suspension with subaerial exposition - soil formation processes in flood plains
				Fc-s_ma_mot	Mudstone massive and mottled	Sediments accumulation by suspension in flood plains / affected by soil formation processes
				Fc-s_ma_var	Mudstone massive and varicolored	Soil formation processes in flood plains

Table 3. — Definition, interpretation, and stratigraphic distribution of the lithofacies associations along the StLs of the Honda Group at the La Venta site.

Lithofacies Association	Basic facies code (Miall 2006)	Stratigraphic level	
		Predominates	Minor proportion
A (Migratory bars and gravitational deposits in meandering channels)	Gh/St/Sl/Sp-St/Sh/Sm/Sp	2/4/6/13/18	1/3/5/7/9/14/16/17
B (Floodplains)	Fl/Fr/Fm/Sh-Fl*	1 (upper part)/3/5/7/9/10/12/14/15/16/17/19	1 (lower part)
C (Crevasse-splay)	Sh/Sm/St/Sr/Fl/Fr	–	1/3/5/9/10/12/14/16/19
D (Braided river bars)	Gmg/Sl-Gt*/Gp	8	–
E (Back swamp / oxbow lake)	Fsm	11	–
F (Flash flood events)	Sh-St/Sh	–	5/7/16
G (Sediment-gravity and hyper-concentrated flows)	Sm/Sh/St/Sm-Gmm	1 (lower part)	–

Age model

Using the information from all the geochronological samples (Fig. 3; Supplementary material, Appendix 8; https://github.com/dsilvestro/agez), we constructed a Bayesian statistical framework to produce a depositional age model with its corresponding credible interval for the entire stratigraphic sequence (Table 4). It was created using available Ar-Ar, ZFT, and Zr U-Pb ages that have been interpreted as the result of syn-sedimentary volcanism (Takemura & Danhara 1985; Flynn *et al.* 1997; Anderson *et al.* 2016). Despite the differences in the closure temperatures and uncertainties of these methods, in this geological context, these ages constrain the depositional age of the La Victoria and the Villavieja formations, which justifies their inclusion in the model.

Given a set of N dated zircons from S samples, we indicated with $z = \{z_1, ..., z_N\}$ the ages of the zircons and with $x = \{x_1, ..., x_S\}$ the ages of the samples. The samples were ordered according on their depth and we assumed their age strictly follows that order such that $x_i > x_{i-1}\}$. We indicated the set of zircons found in a sample s as z^s. The obtained ages (z_i) were assumed to be unknown but linked to its measured age, expressed as a mean μ_i and a standard deviation σ_i. The mean ages μ and a standard deviations σ of all ages represent the input data of the model, which aims to estimate the vector z and the ages of all samples x; because the ages can be measured by different methods (e.g., $m \in \{1, ... , M\}$, namely, in this study: Zr-U-Pb, ZFT, Ar-Ar), the uncertainty around the true age of zircon is assumed to be further affected by how it was measured. We compute the likelihood of the age of the i^{th} sample based on a normal density:

$$P(\mu_i \mid z_i, \sigma_i, \in_m) \sim N(z_i, \sigma_i + \in_m)$$

Where $\in_m$ is the bias in the estimated error of the measurement method m, the parameters z_i and $\in_m$ are considered unknown and jointly inferred from the data using a Markov Chain Monte Carlo (MCMC) algorithm.

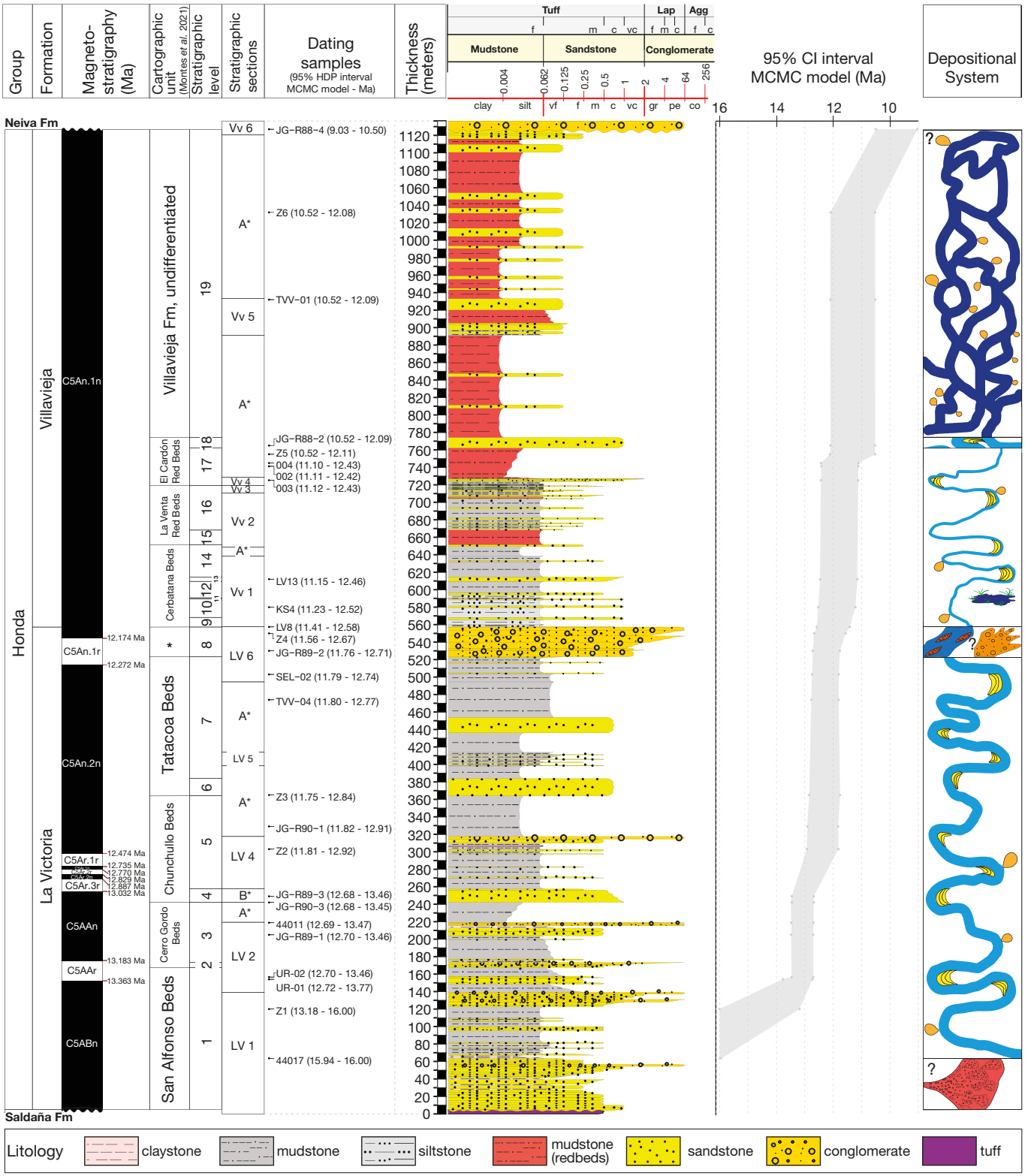

FIG. 3. — Probabilistic age model of the Honda Group at the La Venta site. Reinterpretation of the magnetostratigraphy chrons is based on our age model. The ages of the chrons are based on Hilgen *et al.* (2012). For information about the difference between the probabilistic age model and that of Flynn *et al.* (1997), see Supplementary materials Appendix 15.

Age CI	Age model M	Age model x̄ (Ma)	Strat. position (meters)	StL	Cartographic unit (Montes *et al.* 2021)	Stratigraphic unit
15.94	15.99	15.99	63.5	1	San Alfonso Beds	La Victoria Formation
16.00	15.00	15.99	120			
13.18	13.27	13.27	154			
16.00	15.20	16.00	156.6			
12.72	13.26	13.26	205			
13.77	13.18	13.18	218.8			
12.70	13.72	13.72	242			
13.46	13.77	13.77	249			
12.70	13.11	13.11	303	2	Cerro Gordo Beds	
13.46	13.11	13.11	329			
12.69	13.13	13.13	365	3		
13.47	13.13	13.13	474			
12.68	13.10	13.11	503	4	Chunchullo Beds	
13.45	13.11	13.11	530			
12.68	12.09	12.39	550	5	Tatacoa Beds	
13.46	12.39	12.40	557			
11.81	12.40	12.40	580	6	Cerbatana Conglomerate Beds	
12.92	12.39	12.39	612			
11.82	12.40	12.39	725	7	Cerbatana Beds	
12.91	12.33	12.31	741			
11.75	12.29	12.31	744.9	8	El Cardón Red Beds	
12.84	12.32	12.29	755			
11.80	11.76	12.28	765	9	Villavieja Fm undifferentiated	
12.77	11.79	12.26	932			
11.79	11.56	12.14		10		
12.74	12.71	12.26				
11.76	12.17	12.02		11		
12.71	12.29	11.94				
11.56	12.05	11.88		12		
12.67	11.98	11.92				
11.41	11.88	11.84		13		
12.58	11.23	11.81				
11.15	11.12	11.79		14		
12.46	11.11	11.45				
12.43	11.10	11.44		15		
12.42	10.52	11.48				
10.52	12.43	12.11		16		
12.09	10.52	11.48				
	12.09	11.44		17		
		11.48				
		11.45		18		
		11.44				
		11.44		19		
		11.48				
		10.52				
		12.09				

FIG. 4. — Geochronology dataset of La Venta site. Reinterpretation of the magnetostratigraphy chrons of Flynn *et al.* (1997) is located on the bottom followed by the model age, the CS, and the stratigraphic position of each sample. Geochronology sample references: Takemura *et al.* (1992): 002, 003, and 004; Takemura & Danhara (1985): LV8, KS4 and LV13; Flynn *et al.* (1997): JG-R89-2, JG-R89-3, and JG-R88-2; Anderson *et al.* (2016): Z1, Z2, Z3, Z4 and Z5; Cadena *et al.* (2020): 46311(UR-01) and 46312 (UR-02); Montes *et al.* (2021): SEL-02; this work: 44017, 44011, TVV-04, and TVV-01. The stratigraphic position of geochronology samples was estimated by literature reported information, graphic correlations, and the cartography of Montes *et al.* (2021). Updated polarity chrons is based on our age model and Hilgen *et al.* (2012).

TABLE 4. — Computed ages based on the probabilistic age model of the Honda Group.

Sample name	Stratigraphic position (m)	Estimated age (Ma)		95% CI interval	
		Mean	Median	Young	Old
JG-R88-4	1127	9.95	10.04	9.03	10.50
Unconformity	1126.5	10.50	10.50	10.50	10.50
Z6	1030.9	11.43	11.47	10.52	12.08
TVV-01	932	11.44	11.48	10.52	12.09
JG-R88-2	765	11.44	11.48	10.52	12.09
Z5	755	11.45	11.48	10.52	12.11
004	744.9	11.79	11.82	11.10	12.43
002	741.24	11.81	11.85	11.11	12.42
003	725.2	11.84	11.88	11.12	12.43
LV13	612	11.88	11.92	11.15	12.46
KS4	580	11.94	11.98	11.23	12.52
LV8	557.4	12.02	12.05	11.41	12.58
Z4	550	12.14	12.17	11.56	12.67
JG-R89-2	530	12.26	12.29	11.76	12.71
SEL-02	503	12.28	12.31	11.79	12.74
TVV-04	474	12.29	12.32	11.80	12.77
Z3	365	12.31	12.33	11.75	12.84
JG-R90-1	329	12.39	12.40	11.82	12.91
Z2	303	12.39	12.40	11.81	12.92
JG-R89-3	249	13.09	13.11	12.68	13.46
JG-R90-3	242	13.10	13.13	12.68	13.45
44011	218.8	13.11	13.13	12.69	13.47
JG-R89-1	205	13.11	13.13	12.70	13.46
UR-02	156.6	13.11	13.13	12.70	13.46
UR-01	154	13.27	13.26	12.72	13.77
Z1	120	15.00	15.20	13.18	16.00
44017	63.5	15.99	16.00	15.94	16.00
Maximum age	–	16.00	16.00	16	16.00

The value of x_j, the age of the j^{th} sample, is determined by two latent variables (r_j and I_j) and constrained by sampled values of z such that $z_i > z_{i-1}$ for $i \in \{2, \ldots, S\}$, with i reflecting the relative stratigraphic order of samples from the youngest to the oldest. Specifically, we define as:

$$\zeta_j = \min(z^s), \text{ for } s \in \{j, \ldots, S\}$$

the minimum age across all zircons included in the j^{th} sample and in all older samples. Thus, ζ_j represents the upper (older) boundary for the age of sample j, which must be younger than all following samples (ordered by depth) and then its youngest zircon. Under this notation, we define the age of a sample as:

$$x = \begin{cases} r_j\,(\zeta_j), & \text{if } j = 1 \\ x_j - 1 + r_j(\zeta_j - x_j - 1), & \text{if } j > 1 \end{cases}$$

where $r_j \in (0, 1)$ is an estimated sample-specific latent parameter determining how close x_j is to its lower boundary x_{j-1} (or to 0 if $j = 1$). Thus, when $r_j \approx 0$, the sample's age is close to its younger boundary, and when $r_j \approx 1$, it is close to its older boundary. We also take into account that zircon can be younger than the sample it was found in, for instance, due to a dating error or to uncertainties associated with the dating technique. To account for this possibility, we additionally estimate a vector of identifiers $I = \{I_1, \ldots, I_N\}$ that define which zircons (identified by $I = 1$) are older than the sample and therefore used to determine its upper age boundary and which zircons (identified by $I = 0$) are younger than the age of the sample. Thus, the upper boundary of a sample age is:

$$\zeta_j = \min\,(z_s \setminus I_s^0), \text{ for } s \in \{j, \ldots, N\},$$

Where $z_s \setminus I_s^0$ indicates the subset of zircons in sample s with an indicator equal to 1, i.e. excluding zircons identified as younger than the sample.

We can now define the prior probability of z_i^j, i.e., the i^{th} zircon in sample j as a function of the sample's age (x_j) and an estimated scale parameter s_j. We model the prior distribution of zircons in a sample using a compound-Uniform-Cauchy distribution, defined as:

$$P(z_{i,j} \mid x_j, s_j) = \begin{cases} z_{i,j} \sim \mathcal{U}(0, 2x_j), & \text{if } z_{i,j} < x_j \\ z_{i,j} \sim \mathcal{C}(x_j, s_j), & \text{if } z_{i,j} \geq x_j \end{cases}$$

Where s_j is the sample-specific scale parameter of the Cauchy distribution. Under this parameterization, the age of the zircons identified as younger than the sample will have a prior uniform probability ranging from 0 to the sample's age and rescaled to integrate to 0.5. The other zircons will instead follow a half-Cauchy distribution with a mode equal to the sample's age (detailed information in Supplementary materials, Appendix 9B). We run the age analysis using the ages compiled in Supplementary material Appendix 8B. The Bayesian age model is implemented in the open-source *agez* Python library, available here: https://github.com/dsilvestro/agez.

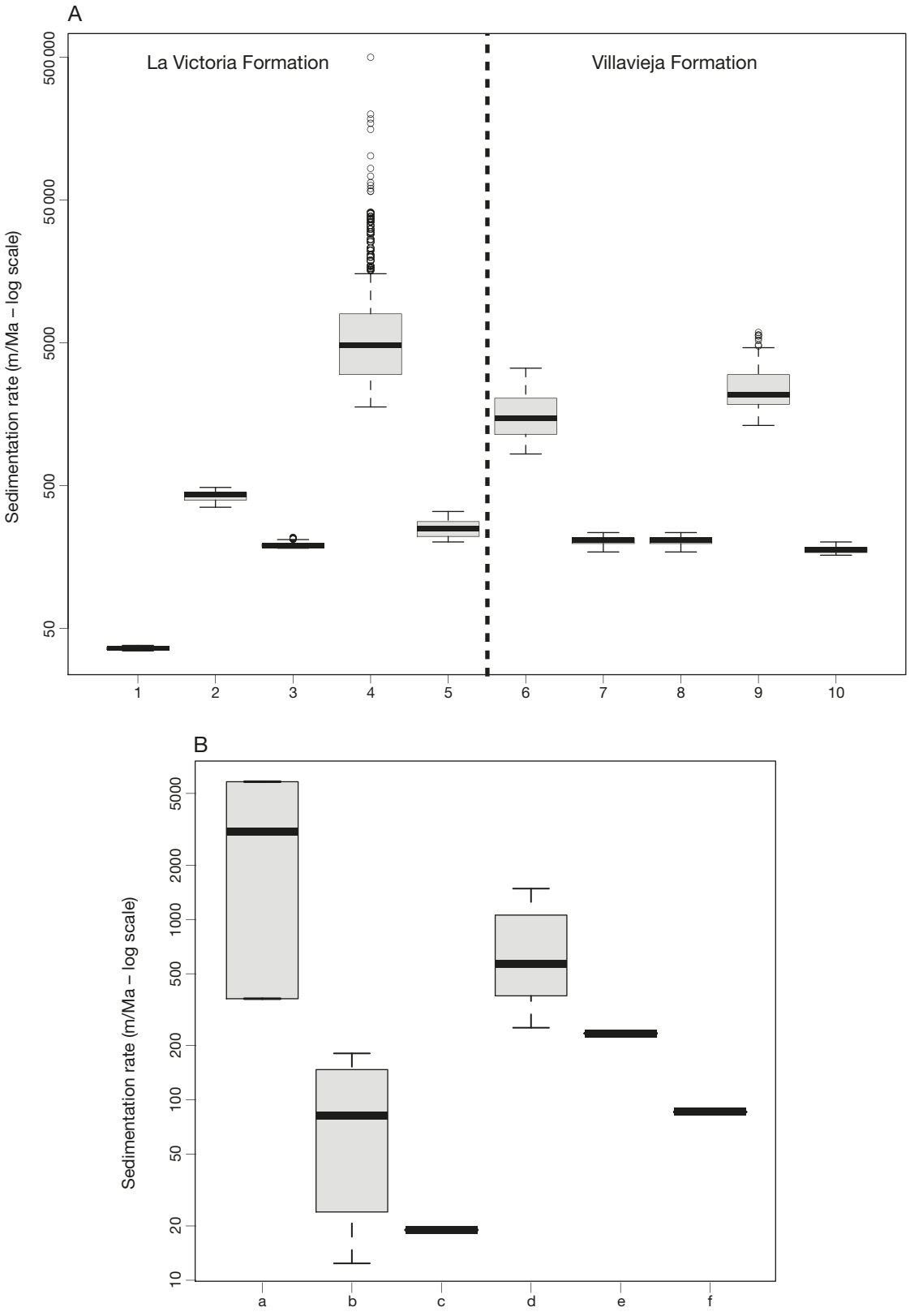

FIG. 5. — Computed sedimentation rates of the Honda Group throughout the La Venta site: **A**, boxplots of sedimentation rates every 100 stratigraphic meters through the La Victoria and the Villavieja formations. Vertical axis is in logarithmic scale; **B**, boxplots of sedimentation rates for each main feature of the depositional settings recorded at the Honda Group in La Venta. Vertical axis is in logarithmic scale. Abbreviations: **a**, overbank deposits with incipient paleosols; **b**, channel sandstone; **c**, overbank deposits without paleosols; **d**, overbank deposits with paleosols; **e**, channel fill and debris flow; and **f**, swamp/lake deposits.

TABLE 5. — Sedimentation rates determined at every 100 meters throughout the Honda Group at La Venta site and sedimentation rates determined for each sedimentary succession interpreted as a main depositional feature of an accumulation system. Abbreviations: **a**, overbank deposits with incipient paleosols; **b**, channel sandstone; **c**, overbank deposits without paleosols; **d**, overbank deposits with paleosols; **e**, channel fill and debris flow; and **f**, swamp/lake deposits.

Segment	Stratigraphic Interval (m)	Sed. rate (m/Ma)	Depositional setting	Stratigraphic Interval (m)	Sed. rate (m/Ma)
10	970-1070	180	d	774.2-1126.5	503.4
9	870-970	2483	b	762.2-774.2	40.7
8	770-870	204.4	d	614.5-762.2	631.8
7	670-770	204.6	b	609.5-614.5	181
6	570-670	1645.8	f	557.2-609.5	85.7
5	470-570	251	e	523.3-557.2	233.6
4	370-470	12630	d	383.8-523.3	1483.3
3	270-370	192.5	b	364-383.8	147.1
2	170-270	424.3	d	257.5-364	251.1
1	70-170	36.3	b	242.2-257.5	123.6
–	–	–	a	173.2-242.2	5804.5
–	–	–	b	167.6 -173.2	23.9
–	–	–	c	139.2-167.6	19
–	–	–	b	122.7-139.2	12.4
–	–	–	a	63.5-122.7	363.7

SEDIMENTATION RATES

We calculated the sedimentary rates along the entire stratigraphic sequence. We run the analysis by dividing the sequence into segments of 100 stratigraphic meters each (Fig. 5A; Table 5). In each segment, we selected at random an age within the confidence envelope of the age model for the stratigraphic level at the base and the top of the interval and proceeded to calculate the sedimentation rate (i.e. the number of stratigraphic meters every one million years). We repeated the same process 300 times for each segment and calculated the mean that was used as representative for the sedimentation rate of the segment (Fig. 5A; Table 5). Each iteration must respect a simple rule; the top must be younger than the base. We also performed the same procedure for the computation of the sedimentation rate of each main feature of the depositional setting (Fig. 5B; Table 5).

FOSSIL LOCALITIES

We compiled all fossil localities reported in the literature and placed each of them on the updated geological map of the region (Montes *et al.* 2021; Fig. 1). Furthermore, we determined their stratigraphical position in our CS for each locality, its corresponding lithofacies associations, and age model (Supplementary materials, Appendix 10). We excluded fossil localities that were recorded on maps but not located within any of the Stratigraphic Levels (StLs) or lacked a sedimentary column that could be correlated to (e.g., locality TW-2 reported by Watanabe *et al.* 1979; or locality 94 reported by Guerrero 1997; detailed information in Supplementary materials, Appendix 10). Then, we placed the fossil localities on the geological map of Montes *et al.* (2021) by georeferencing the geological maps of Fields (1959), Watanabe *et al.* (1979), Takemura (1983), Takemura & Danhara (1985), Takai *et al.* (1992, 2001), and Guerrero (1997) using QGIS (2020, version 3.10.2; Supplementary materials Appendix 5). We created shape files that includes locality number, source (map's author), locality name, and location (geographical coordinates). The same procedure was used to integrate the chronostratigraphic samples (previously reported and those studied here) and the stratigraphic sections (previously reported and those measured by us; Fig. 1). We used the graphic correlation method (Shaw 1964) to place the fossil localities in the CS and included Guerrero's (1997) key stratigraphic levels (StLs; i.e., Cerro Gordo Sandstone Beds, Chunchullo Sandstone Beds, Tatacoa Sandstone Beds, Cerbatana Conglomerate Beds, Monkey Beds, Fish Bed, Ferruginous Beds, La Venta Red Beds, El Cardón Red Beds, Sand Francisco Sandstone Beds, and Polonia Red Beds; Supplementary material Appendix 13). This step allowed us to determine the stratigraphic position in space (i.e., lithofacies association) and time (i.e., meters, StLs, and geochronological samples) for all reported fossil localities (Fig. 2 and Supplementary material Appendix 11). Localities that lacked geographic positions (e.g., locality V-5046 from McDonald 1997) or are beyond the boundaries of Montes *et al.* (2021) map were excluded from the analysis (for detailed information, please see Supplementary material Appendix 10).

All the geological information including sections, cartography, samples with geochronology, and sites with fossils are compiled in a GIS project using an open-source product (QGIS), that can be easily used in future projects (Supplementary material Appendix 5).

RESULTS

LA VENTA COMPOSITE STANDARD SECTION

We established a CS of the Honda Group that measured 1121.5 m, 552.2 m stratigraphic meters corresponding to the La Victoria Formation and 569.3 m to the Villavieja Formation (Fig. 2 and Supplementary material Appendix 6). The CS includes 19 stratigraphic levels (StLs), eight in the La Victoria Formation and 11 in the Villavieja Formation which correspond to those previously defined by Guerrero

FIG. 6. — Field photographs: **A**, grey conglomeratic litharenite, friable, with clasts of quartzite, chert, and Saldaña's fragments; **B**, grey litharenite, with cross-stratification and abundant calcareous concretions; **C**, red and grey varicolored mudstone with calcareous (caliche) nodules; **D**, panoramic view of mudstone beds and incipient paleosols; **E**, Mini Desierto site, red plane parallel mudstone beds interbedded with conglomeratic lenticular beds; **F**, panoramic view of El Cardón Red Beds. Abbreviations: **Ccs 0**, conglomerate clast-supported; **(c)S**, conglomeratic sandstone; **S**, sandstone; **S(vf)**, sandstone with very fine grain size; **Fc-s**, fine claystone – siltstone. Lines: **dashed red lines**, beds; **dashed white lines**, cross-stratification. For a detailed stratigraphic section of the Mini Desierto site, see Supplementary materials, Appendix 12. Scale bars: A, C, 15 cm; B, 20 cm.

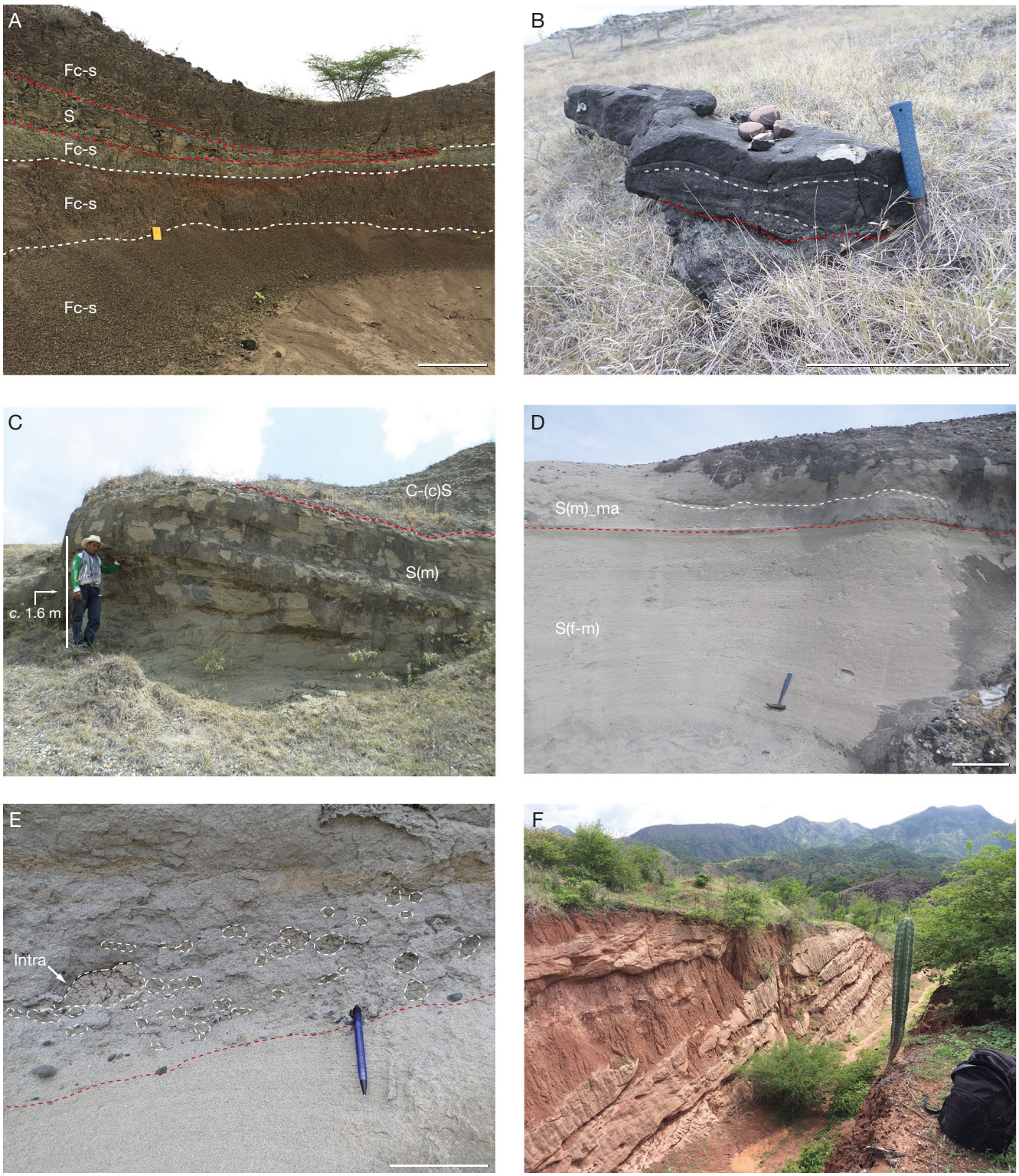

FIG. 7. — Field photographs: **A**, grey sandstone bed, lenticular-shaped (dashed red lines) within red and grey mudstone (dashed white lines); **B**, soft deformation (dashed white lines), fluids supersaturated result of crevasse-splay event; **C**, lower boundary of Cerbatana Conglomerate Beds (dashed red line); **D**, very thick medium-grained sandstone bed with pseudo lamination overlaid by massive sandstone bed; **E**, sandy mudstone bed (base; dashed red line) overlaid by a medium-grained sandstone bed with abundant mud intraclasts (dashed white lines) which, at the bottom, are organized by density – the sand fraction has sub-angular to angular particles, well-sorted but compositionally immature; **F**, panoramic view of Morrongo site – red mudstone interbedded with grey litharenite channels, gently dipping to the NW. Abbreviations: **Ccs 0**, conglomerate clast-supported; **(c)S**, conglomeratic sandstone; **S**, sandstone; **S(vf)**, sandstone with very fine grain size; **Fc-s**, fine claystone – siltstone. Scale bars: A, 1 m; B, 40 cm; D, 50 cm; E, 15 cm.

TABLE 6. — Data matrix of fossil localities occurrences along the different StLs and the determined lithofacies associations throughout the Honda Group at the La Venta site.

Stratigraphic Level	Lithofacies Association							
	A	B	C	D	E	F	G	NA
1	2	2	0	0	0	0	3	0
2	2	0	0	0	0	0	0	0
3	8	21	0	0	0	0	0	1
4	2	0	0	0	0	0	0	0
5	5	44	0	0	0	2	0	1
6	1	0	0	0	0	0	0	0
7	3	14	0	0	0	0	0	0
8	0	0	0	2	0	0	0	0
9	0	40	4	0	0	0	0	11
10	0	8	0	0	0	0	0	0
11	0	0	0	0	8	0	0	8
12	0	6	1	0	0	0	0	0
13	1	0	0	0	0	0	0	0
14	1	2	1	0	0	0	0	0
15	0	3	0	0	0	0	0	0
16	3	4	0	0	0	0	0	0
17	0	3	0	0	0	0	0	2
18	1	0	0	0	0	0	0	0
19	0	7	1	0	0	0	0	0
NA	0	0	0	0	0	0	0	24

(1997). The stratigraphic succession contains 39 lithofacies (Table 2 and Supplementary materials Appendices 6; 7), in seven lithofacies associations (A to G) along the sedimentary succession of the Honda Group (Fig. 2; Table 3).

LITHOFACIES ANALYSIS

The most common lithofacies association is B (in 154 levels, Table 3, Supplementary materials Appendix 10), followed by lithofacies association A (29; Table 3; Supplementary materials, Appendix 10), which correspond to accumulation in confined fluvial systems and its adjacent floodplain. Lithofacies association A is more frequent in the La Victoria Formation (76.3%) than the Villavieja Formation (23.7%) (Table 3, Supplementary materials Appendix 10). It suggests a depositional system driven by migratory bars and gravitational deposits in meandering channels (Allen 1982; Reineck & Singh 1986; Miall 1992, 2006) (Fig. 6A, B). Lithofacies association B is close to be equally present in the La Victoria and the Villavieja formations, 43.6% and 56.4%, respectively (Figs 6C-F; 7A; Table 3). It reflects environmental systems where sediment accumulation occurred by suspension in low energy floodplains (resulting in a vertical aggradation pattern), which may include signs of reducing conditions (mudstones with red-gray drab colors), incipient soil formation processes (mottled and varicolored churned textures) that indicate variations in the water table, and well-developed paleosols resulting from oxidizing conditions produced by long-term subaerial exposure and weathering (red beds) (Einsele 2000; Miall 2006). Lithofacies association C (unconfined sediment gravity flow) is more common in the Villavieja than in the La Victoria Formation, 89.7 vs 10.3%, respectively (Table 3). It may result from sediments accumulated by hyper-concentrated flows (occasionally affected by undulating currents) because of large unconfined overflows and crevasse-splay processes in the floodplain, where breaks may occur showing evidence of dewatering, soft-sediment deformation (Fig. 7B), intense bioturbation, subaerial exposure, and soil formation processes (Einsele 2000; Middleton 2003; Miall 2006).

Lithofacies association D, corresponds to confined braided fluvial systems and it is present only in the La Victoria Formation, Cerbatana Conglomerate Beds, StL 8 (Fig. 7C; Table 3). This association displays crossbedding, massive or crudely bedded sediment, and clast-supported gravel (Einsele 2000). Sediments of this lithofacies accumulated in a setting of braided rivers with transverse bedforms, deltaic growths from older bar remains, and clast-rich debris-flow or pseudo-plastic debris flow (Miall 2006). Lithofacies association E corresponds to a lacustrine setting and is only found in the Villavieja Formation Fish Bed, StL 11 (Table 3). Sedimentation occurred by suspension in a reducing environment like back swamp or oxbow lake (Miall 2006), which preserves remains of fish, mammals, amphibians, birds, crocodiles, snakes, and coprolites. Lithofacies association F (volcanic-related gravity flow) is more frequent in the La Victoria than in Villavieja Formation, 78.7% vs 21.3% respectively (Fig. 7D, E; Table 3). It could be the product of ephemeral flows related to flash flood events under upper-plane bed conditions (Miall 2006) and the occurrence of volcanoclastic deposits described by Guerrero (1997) and Montes *et al.* (2021). Lastly, lithofacies association G (unconfined sediment gravity flow) is found only in the La Victoria Formation Bed set below Cerro Gordo, StL 1 (Table 3). It could be a product of rapid accumulation by sediment-gravity flow, hyper-concentrated flows under upper plane bed conditions (associate to unconfined flash flows), and to a small extent plastic debris flows and occasional channel structures (Fig. 7F) (Miall 2006; Einsele 2000).

U-PB GEOCHRONOLOGY

Sample 44017, located at meter 63.5 in the La Victoria Formation, is a volcanic-rich arenite and has a youngest statistical population (YSP) of 17.6 ± 0.4 and a youngest detrital zircon (YDZ) of 17.6 ± 0.8, based upon 105 single zircon ages, including five age populations, with significant age peaks *c.* 18 Ma, 46 Ma, 82 Ma, and 99 Ma and minor ages > 200 Ma. Sample 44011, located at meter 218.8 in the La Victoria Formation, is a volcanic-rich arenite and has a YSP of 13.9 ± 0.3 Ma and a YDZ of 13.8 ± 0.6 Ma based on 92 single zircon ages, including four-age populations, with significant age peaks *c.* 14 Ma, 40 Ma, 84 Ma, 186 Ma, and minor ages distributed > 250 Ma. Sample TVV-04, located at meter 474 in the La Victoria Formation, is a lithic sandstone with reworked pyroclastic material that has a YSP of 12.8 ± 0.1 Ma and a YDZ of 12.8 ± 0.2 Ma based on 104 single zircon ages, including six-age populations, with significant age peaks *c.* 13 Ma, 33-40 Ma, 84 Ma, minor ages peaks *c.* 187 Ma, 232 Ma, and 961 Ma; minor ages correspond to ages <1000 Ma. Sample TVV-01, located at meter 932 in the Villavieja Formation, is a quartzarenite and has a YSP of 80.9 ± 2.5 Ma and a YDZ of 12.9 ± 0.4 Ma based on 104 single zircon ages, including four-age populations, with significant age peaks *c.* 183 Ma and 272 Ma and minor ages peaks *c.* 81 Ma and 1521 Ma; minor ages include ages >1500 Ma.

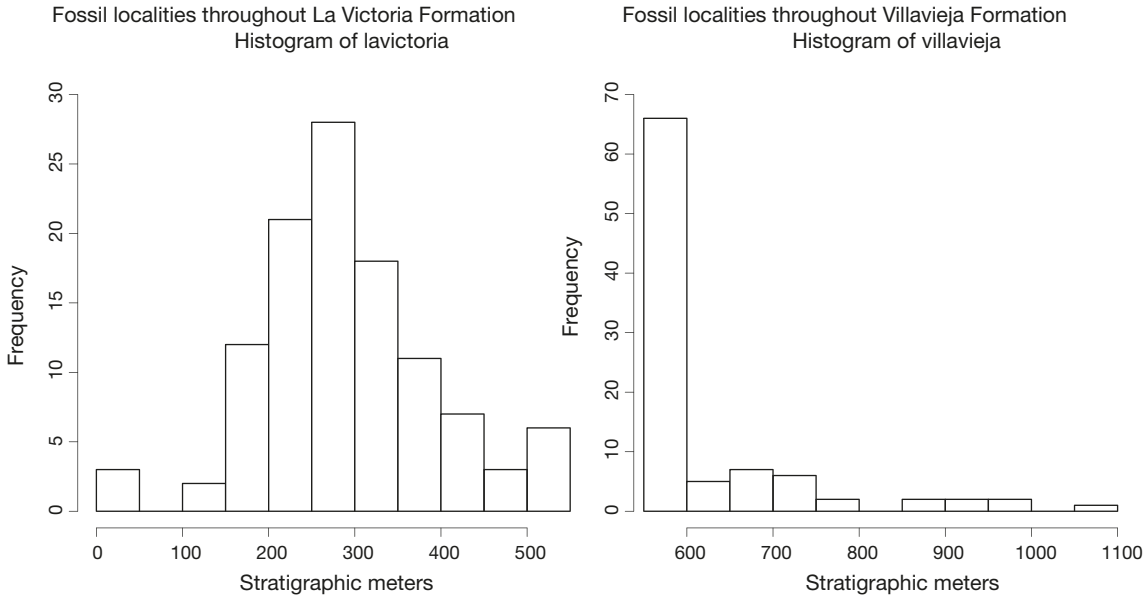

Fig. 8. — Stratigraphic distribution of fossil localities for the La Victoria and Villavieja formations.

Age model

Based on the 95% credible intervals estimated by our Bayesian framework (Table 4), our age model suggests that the Honda Group at La Venta extends from 16-15.94 Ma at meter 63.5 in the CS (Fig. 3) to 10.62 to 10.50 Ma at meter 1120 in the CS (Fig. 3). Specifically, the span of the La Victoria Formation is from 16-15.94 Ma to 12.58-11.41 Ma; meters 63.5 and 557.4 respectively in the CS (Fig. 3), and that of the Villavieja Formation from 12.58-11.41 Ma to 10.62-10.50 Ma; meters 557.4 to 1120 (Fig. 3). There is an unconformity between the Villavieja and Neiva formations at meter 1126.5 that started at 10.5 Ma (Fig. 3; Table 4).

Sedimentation rates

Mean sedimentation rate for the La Victoria Formation is 2706.8 m/Ma, with a minimum value at segment 1 (36.3 m/Ma; 70 to 170 stratigraphic meters; Fig. 5A; Table 5) and the maximum value at segment 4 (12630 m/Ma; 370 to 470 meters; Fig. 5A; Table 5). There is a major increase in the sedimentation rate at the middle part of the La Victoria Formation, from segments 1-2 (mean sedimentation rate 230.3 m/Ma) to segments 3-5 (mean sedimentation rate 4357.7 m/Ma). Mean sedimentation rate for the Villavieja Formation is 943.1 m/Ma with a minimum at segment 10 (180 m/Ma; 970 to 1070 meters; Fig. 5A; Table 5) and a maximum at segment 9 (2483 m/Ma; 870 to 970 meters in the CS; Fig. 5A; Table 5). The sedimentation rates of the upper La Victoria Formation (segments 3, 4, and 5) and the Villavieja Formation are not significantly different (segments 6, 7, 8, 9, and 10; $t = 0.82015$, *p-value* = 0.5).

The depositional setting with highest sedimentation rates is the overbank deposit with incipient paleosols, which have a mean sedimentation rate of 3084.1 m/Ma (Max.: 5804.5 m/Ma. Min.: 363.7 m/Ma; Fig. 5B; Table 5). Next highest rate is overbank deposits with paleosols, which have a mean sedimentation rate of 717.4 m/Ma (Max.: 1483.3 m/Ma. Min.: 251.1 m/Ma; Fig. 5B, Table 5). Channel fill and debris flow deposit at the Cerbatana Conglomerate Beds (meters 523.3 to 557.2) have a sedimentation rate of 233.6 m/Ma (Fig. 5B, Table 5). Swamp/lake deposit (meters 557.2 to 609.5) shows a sedimentation rate of 85.7 m/Ma (Fig. 5B, Table 5). Channel sandstone environments have a mean sedimentation rate of 82.15 m/Ma (Max.: 181 m/Ma. Min.: 12.4 m/Ma). The lowest sedimentation rate is in overbank deposits without paleosols (meters 139.2 to 167.6), with a rate of 19 m/Ma (Fig. 5B, Table 5).

Fossil localities

There are 251 fossil localities reported in the literature (Supplementary material, Appendix 10). We were able to geographically locate 202 of them; 178 were also located in Montes *et al.*'s (2021) geological map (94 from La Victoria, 84 Villavieja; Fig. 1 and Supplementary materials, Appendices 5, 6, 10, 11; the remaining 24 localities are beyond the boundaries of Montes *et al.*'s (2021) map). We established the stratigraphic position in the CS as well as the lithofacies associations for 205 fossil localities, 111 from the La Victoria Formation and 94 from the Villavieja Formation (Fig. 8; Table 6; Supplementary material, Appendix 10) while 47 localities did not report a stratigraphic position (e.g., locality V-5046 in McDonald 1997; details in Supplementary material Appendix 10).

The stratigraphic interval in the La Victoria Formation with the highest number of fossil localities (60%) is between 200 to 350 meters (67 localities, Fig. 8, and Supplementary material Appendix 10), whereas in the Villavieja Formation is between 559 to 600 meters (70%, 66 localities, Fig. 8, and Supplementary material Appendix 10).

The StLs with the highest number of fossil localities include StLs 9 (55), StLs 5 (52), and StLs 3 (30) (Table 6). Seventy-five percent of all fossil localities were found in lithofacies associa-

tion B (81 in La Victoria and 73 in Villavieja), followed by 14% in lithofacies association A (23 in La Victoria and 6 in Villavieja), and the remaining 10% were found in all other lithofacies associations (22) (Table 6).

DISCUSSION

Accumulation systems

Our results suggest that the lowermost 60 stratigraphic meters of the La Victoria Formation were dominated by sediment-gravity and hyper-concentrated flows interbedded by river migratory bars and floodplains (lithofacies associations G and B; Fig. 2). This type of depositional system could be found in the distal facies of an alluvial fan (Miall 2006; Einsele 2000) or a "terminal fan" in the distributary zone (Kelly & Olsen 1993; Miall 2006), associated with the scarp's backstepping, relief (reduction in the uplands) and progradation due to uplift or subsidence in the basin (fining- and coarsening-upward successions, respectively; Einsele 2000). The overlying succession, from stratigraphic meters 60 to 530, is dominated by a fluvial meandering system (Fig. 2), with sediment accumulated in migratory bars, gravitational deposits due to bank instability, bioturbated sandstones, and chute bars, some reflecting lateral accretion packages of meandering belts (lithofacies association A, StLs 2, 4, and 6) with thickness *c.* 10 to 17 m that record the basal boundaries of Montes *et al.*'s (2021) cartographic units II, III, and IV (Fig. 1 and Supplementary material, Appendix 13). Those levels alternate with floodplains deposits (resulting in a vertical aggradation pattern) with pedogenesis influenced by crevasse-splay processes (lithofacies association B and C in StLs 1, 3, 5, and 7) and flash-floods in upper flow regime (lithofacies association F). Drab color paleosols of the La Victoria Formation may suggest a poorly drained floodplain that was seasonally flooded (Salazar-Jaramillo *et al.* 2022) and could indicate a shorter weathering time (Miall 2006). The whole succession suggests a gravel-sand meandering fluvial system (Allen 1982; Reineck & Singh 1986; Einsele 2000; Miall 1992, 2006) influenced by volcanoclastic processes (Guerrero 1997; Flynn *et al.* 1997) that could be associated to the Cauca-Patía magmatic center (Montes *et al.* 2021).

The top level of the La Victoria Formation (level 8, the Cerbatana conglomerate, 40 stratigraphic meters) is dominated by conglomerate transverse bedforms, deltaic growths from older bar remains, clast-rich debris flow, and pseudoplastic debris flow (lithofacies association D). The lithofacies association may suggests a braided river system influenced by debris flows and catastrophic floods events (Einsele 2000; Miall 2006), as previously interpreted by Wellman (1970), Takemura (1983), Takai *et al.* (1992), Villarroel *et al.* (1996), and Guerrero (1997). However, this unit also has polymictic clasts, including black chert, quartz, and volcanic fragments (Guerrero 1997, and this work Supplementary material, Appendices 7; 14), that may suggest reworking of Paleogene age units from nearby, intrabasinal sources (e.g., Gualanday Group, Bayona *et al.* 2009). Therefore, a shift in source material to unconsolidated conglomerate beds could also produce a conglomerate level without a significant change in the fluvial system.

The lower 200 stratigraphic meters of the Villavieja Formation are dominated by sandy channel bars and fill (StLs 13 and 18, lithofacies association A), floodplains with crevasse-splay deposits (lithofacies association B and C, respectively in StLs 9, 10, 12, 14, and 16), conspicuous red-beds in well-developed paleosols (StLs 15 and 17) suggesting long-term subaerial exposition, and lake or back swamp settings (lithofacies association E in StL 11) (Fig. 2). The accumulation system could be related to a sand-bed meandering river (Reineck & Singh 1986; Einsele 2000; Middleton 2003; Miall 2006) as has been proposed before (Fields 1959; Villarroel *et al.* 1996; Guerrero 1997). Above *c.* 774 m, the stratigraphic succession in the Villavieja Formation (StL 19; Fig. 2) is dominated by the sedimentary accumulation of particles in suspension, hyper-concentrated flows, and intense pedogenesis represented by reddish paleosols (lithofacies association B), accumulated in floodplain settings (Miall 2006) that could be part of the anastomosed river system as proposed by Guerrero (1997).

Age model and Laventan zone

Using the sedimentary succession described here at La Venta (Madden *et al.* 1997a), we define the Laventan South American mammal zone as the span from 13.8 to 11.8 Ma. The age model presented here supports this scheme, as most of Villavieja/La Victoria accumulated during this interval (Fig. 3, from meter 140 to 1040). The magnetostratigraphy model developed by Flynn *et al.* (1997) agrees with our model age at the base and top of the sequence (chrons C5ABn to C5An. 1n, respectively). However, our interpretation of the chrons within the sequence differs from Flynn *et al.*'s (1997) interpretation, which indicates younger ages than those derived from our age model (Supplementary materials, Appendix 15). Therefore, we have produced a reinterpretation of the polarity sequence described by Flynn *et al.* (1997) that agrees with the chronology of intervals C5An.1n-C5ABn (Hilgen *et al.* 2012) and fits with the mean ages predicted by our probabilistic age model (Figs 3; 4). Specifically, in the chron C5ABn, our reinterpretation locates the StLs 1, 2, 3, and lower part of 4, which correlate to Montes' *et al.* (2021) cartographic units San Alfonso Beds, Cerro Gordo Beds, and the lowermost part of Chunchullo Beds. StLs upper parts of 4, 5, and 6 are included in chrons C5Aar, C5AAn, C5Ar.3r, and C5Ar.2n. This interval correlates to the cartographic units Cunchullo Beds and lower Tatacoa Beds (Montes *et al.* 2021). Chrons C5Ar.2r, C5Ar.1n, and C5Ar.1r represent StLs 7, 8, 9, 11, and 12. These correlate to the middle-upper part of Tatacoa Beds, Cerbatana Conglomerate Beds, and the lower part of Cerbatana Beds cartographic units (Montes *et al.* 2021). Chrons 5An.2n, C5An.1r, and C5An.1n include StLs 13, 14, 15, 16, 17, 18, and 19, which correlate with upper Cerbatana Beds, La Venta Red Beds, El Cardón Red Beds, and Villavieja Formation Undifferentiated cartographic units (Montes *et al.* 2021).

Sedimentation rates, tectonics, and climate

There is a significant increase in the mean sedimentation rate from the lower 150 stratigraphic meters of the La Victoria Formation (36.3 m/Ma) to its upper part (4415.6 m/Ma). This significantly higher mean sedimentation rate continued into the Villavieja Formation (up to 2483 m/Ma) (Figs 3; 5A; Table 5). This intraformational difference among sedimentation rates could be the result of a shifting tectonic regime from non/low-subsidence to high-subsidence in the Neiva Basin *c.* 13 Ma (Montes *et al.* 2021). This time interval coincides with the beginning of the southward propagation of the southernmost tip of the Eastern Cordillera and closure of the Serravallian trans-Andean passage (Montes *et al.* 2021), which could enhance the generation of accommodation space driven by high subsidence. Furthermore, the change between sediment-gravity and hyper-concentrated flows interbedded by river migratory bars and floodplains (lower part of the La Victoria Formation) to a fluvial meandering system characterized by lateral accretion alternated with floodplains and pedogenesis (middle and upper part of the La Victoria Formation) also supports a shifting subsidence regime.

The mean sedimentation rates of the middle-upper part of the La Victoria Formation and the Villavieja Formation do not differ significantly. These two segments of the Honda Group therefore accumulated under a high-subsidence regime in the basin until 10.5 Ma, when the angular unconformity between the Honda Group and Neiva Formation is recorded (Figs 2; 3).

Only the first 200 stratigraphic meters of the Villavieja Formation are dominated by an accumulation system homogeneous with the middle-upper part of the La Victoria Formation (a sand-bed meandering river). At *c.* 774 m (*c.* 11.3 Ma), the stratigraphic succession in Villavieja Formation changed to an anastomosed river system dominated by floodplain settings with reddish paleosols. This shift could be explained by three alternative hypotheses: 1) an increase in the landscape slope, which would have enhanced avulsion by a topographic mechanism (Makaske 2001); 2) a shift in sediment source from distal to proximal, that would allow anastomosis by high sediment supply (Makaske 2001); and 3) a drier landscape, which would have enhanced anastomosis by the loss of channel-flow capacity owing to in-channel fluvial deposition (Makaske 2001).

The tectonic hypotheses 1 and 2 could have been structures such as La Becerra Anticline (Montes *et al.* 2021) and the closure of the Serravallian trans-Andean passage (Montes *et al.* 2021), respectively. The global climatic cooling trend during the Miocene (Zachos *et al.* 2001, 2008) may have enhanced the drier conditions of the region (hypothesis 3).

Fossil assemblages

The fossil assemblage includes rodents, primates, armadillos, bats, sloths, astrapotheres, marsupials, cetaceans, litopterns, notoungulates, sirenians, fishes, crocodilians, turtles, squamates, amphibians, birds, crabs, pollen, and wood (Supplementary materials Appendices 13 and 14 for a list of all paleontological publications using material from the La Venta region). There are more fossil reports from the Villavieja Formation than La Victoria (Madden *et al.* 1997a), but the difference is probably due to a more intense exploration of the southern part of La Venta where most of the outcrops belong to the Villavieja Formation (e.g., Fields 1957); in contrast, the La Victoria Formation, which outcrops mostly in the north, still remains unexplored (Dumont & Bown 1997; Flynn *et al.* 1997; Kay & Madden 1997a, b; Guerrero 1997; Hecht & LaDuke 1997; Walton 1997). Most fossil localities are reported from levels StL 9 (Villavieja Formation) and StL 5 (La Victoria Formation) with 54 and 52 fossil localities, respectively, and 84 of them were collected in overbank settings (Table 5).

Fossil records derive from several lithofacies associations, and up to date there is no relation between lithofacies association and the number of fossil localities (Table 6 and Supplementary material, Appendix 16). Nevertheless, many fossil sites have been found in lithofacies associations B, A and D, which correspond to accumulation in confined fluvial systems and their adjacent floodplains. Fossils in association B, which accumulated in meandering rivers probably had minimum transport and could represent an *in-situ* community; of the three lithofacies associations, B has the lowest-energy conditions for sediment accumulation (Kidwell & Flessa 1996), with minimal bioclasts transport (Behrensmeyer 1990). It includes crocodile skulls found in life-position (Langston & Gasparini 1997) and rodent skeletons trapped in burrows (Guerrero 1997). Fossils in association A and D, which accumulated along channel-lag and cannel-bar deposits (i.e., StLs 2, 4, 6, 8, 13, and 18) could have some degree of transport given that particles with weights under 100 grams could move from various meters to several thousand of meters in a meandering system (Behrensmeyer 1988; Aslan & Behrensmeyer 1996). Besides, these fossil assemblages may also suggest a basin-wide faunal source given that the La Venta site has an approximate area of 380 km^2 (Montes *et al.* 2021).

The overbank deposits of the La Victoria Formation have partially mottled horizons and dark red beds, which suggests short times of atmospheric exposure and consequently a minor degree of pedogenesis (Miall 2006); this may have favored the excellent bone preservation in many of the specimens found at La Venta. However, additional studies are required to fully understand the taphonomic processes at La Venta and whether they changed along the stratigraphic profile, lithofacies associations, or depositional system.

CONCLUSIONS

The La Victoria Formation is dominated by a gravel-sand meandering fluvial system whereas the Villavieja Formation is dominated by a sand-bed meandering river system and an anastomosing river system. The shift in accumulation regimes in the Villavieja Formation could have been forced by tectonics and/or climate changes.

The Honda Group spans 5.5 million years, from *c.* 16 Ma to *c.* 10.5 Ma, with most the accumulation occurring between 13.8 and 11.8 Ma.

The La Venta site is still in the early phases of study, and extensive areas, specially to the north, have yet to be fully explored. Furthermore, additional paleobiological, taphonomic, biogeographic, and population-level studies are required to fully understand the ecosystem preserved in the strata of the Honda Group.

Roughly 91% of all paleontological studies at La Venta have focused on taxonomy and systematics, but little effort has been done to understand the evolutionary tempo and mode along the *c.* 5.5 million years that span its stratigraphic succession. Our contribution has placed all the fossil localities studied at La Venta into a single stratigraphical framework allowing us to establish the space and time of every specimen collected, and thereby opening the window to a new generation of studies at La Venta, as have been done at other lagerstätten sites (e.g., the Bighorn Basin).

Acknowledgements
Proyectos Internos Scholarship Universidad EAFIT, the Smithsonian Tropical Research Institute (STRI), the Anders Foundation, 1923 Fund and Gregory D. and Jennifer Walston Johnson supported this research. DS received funding from the Swiss National Science Foundation (PCEFP3_187012) and from the Swedish Research Council (VR: 2019-04739). Author contributions: LM, AC, CJ, contributed to the project planning and writing of this paper. CJ and DS contributed to the elaboration of the Bayesian age model. LM, AC, GB, and FM contributed to the sedimentological analysis. GB, SZ, FM, CJ, AC, LM, SJ, VV, and MI, contributed to geochronology analysis and interpretation. CS and JM, contributed to the measurement and description of stratigraphic sections. Authors acknowledge Semillero de Paleontología Universidad EAFIT. Reviewers Camilo Montes and Alfredo Carlini improved the quality of this manuscript.

REFERENCES

Allen J. R. L. 1982. — *Sedimentary Structures, their Character, and Physical Basis*. Vol. 2. Elsevier, Amsterdam, 663 p. (Developments in Sedimentology; 30B).

Anderson V., Horton B., Saylor J., Mora A., Tesón E., Breecker D. & Ketchan R. 2016. — Andean topographic growth and basement uplift in southern Colombia: Implications for the evolution of the Magdalena, Orinoco, and Amazon river systems. *Geosphere* 12 (4): 1-22. https://doi.org/10.1130/Ges01294.1

Aslan A. & Behrensmeyer A. K. 1996. — Taphonomy and time resolution of bone assemblages in a contemporary fluvial system: The East Fork River, Wyoming. *Palaios* 11 (5): 411-421. https://doi.org/10.2307/3515209

Bayona G., Lamus F., Jiménez G., Rico J., Sierra D., Rosero A. & Montes C. 2009. — Conteo de clastos como metodología en el reconocimiento de unidades conglomeráticas en el Valle Superior del Magdalena (VSM). *Memorias del XII Congreso Colombiano de Geología, Paipa – Boyacá*: T005-R141.

Bayona G. 2018. — El inicio de la emergencia en los Andes del norte: una perspectiva a partir del registro tectónico-sedimentológico del Coniaciano al Paleoceno. *Revista de la Academia Colombiana de Ciencias Exactas, Físicas y Naturales* 42 (165): 364-378. https://doi.org/10.18257/raccefyn.632

Behrensmeyer A. K. 1988. — Vertebrate preservation in fluvial channels. *Palaeogeography, Palaeoclimatology, Palaeoecology* 63: 183-199. https://doi.org/10.1016/0031-0182(88)90096-X

Behrensmeyer A. K. 1990. — Bones, *in* Briggs D. & Crowther P. (eds), *Palaeobiology A Syntesis*. Blackwell Scientific Publications, Oxford: 332-335.

Behrensmeyer A. K. & Hook R. W. 1992. — Paleoenvironmental contexts and taphonomic modes in the fossil record, *in* Behrensmeyer A. K., Damuth J. D., Dimichele W. A., Potts R., Sues H.-D. & Wing S. L. (eds), *Terrestrial Ecosystems Through Time. The Evolutionary Paleoecology of Terrestrial Plants and Animals.* University of Chicago Press, Chicago: 15-136.

Borrero C., Pardo A., Jaramillo C. M., Osorio J. A., Cardona A., Flores A., Echeverri S., Rosero S., García J. & Castillo H. 2012. — Tectonostratigraphy of the Cenozoic Tumaco forearc basin (Colombian Pacific) and its relationship with the northern Andes orogenic build up. *Journal of South American Earth Sciences* 39: 75-92. https://doi.org/10.1016/j.jsames.2012.04.004

Butler J. 1942. — Geology of Honda District, Colombia. *Bulletin of the American Association of Petroleum Geology* 26 (5): 793-837. https://doi.org/10.1306/3D93346C-16B1-11D7-8645000102C1865D

Cadena E., Jaramillo C., Vanegas A., Cottle J. & Johnson T. 2020. — A new Miocene turtle from Colombia sheds light on the evolutionary history of the extant genus *Mesoclemmys* Gray, 1873. *Journal of Vertebrate Paleontology* 39 (5): 1-11. https://doi.org/10.1080/02724634.2019.1716777

Carrillo J. D., Forasiepi A., Jaramillo C. & Sánchez-Villagra M. R. 2015. — Neotropical mammal diversity and the Great American Biotic Interchange: spatial and temporal variation in South America's fossil record. *Frontiers in Genetics – Evolutionary and Population Genetics* 5 (451): 1-11. https://doi.org/10.3389/fgene.2014.00451

Chang Z., Vervoort J. D., Mcclelland W. C. & Knaack C. 2006. — U-Pb dating of zircon by LA-ICP-MS. *Geochemistry, Geophysics, Geosystems* 7: 1-14. https://doi.org/10.1029/2005GC001100

Coutts D. S., Matthews W. A. & Hubbard S. M. 2019. — Assessment of widely used methods to derive depositional ages from detrital zircon populations. *Geoscience Frontiers* 10 (4): 1421-1435. https://doi.org/10.1016/j.gsf.2018.11.002

Dickinson W. R. & Gehrels G. E. 2009. — Use of U-Pb ages of detrital zircons to infer maximum depositional ages of strata: a test against a Colorado Plateau Mesozoic database. *Earth and Planetary Science Letters* 288 (1-2): 115-125. https://doi.org/10.1016/j.epsl.2009.09.013

Dumont E. & Bown T. M. 1997. — New Caenolestoid Marsupials, *in* Kay R. F., Madden R. H., Cifelli R. L. & Flynn J. J. (eds), *Vertebrate Paleontology in the Neotropics. The Miocene Fauna of La Venta, Colombia*. Smithsonian Institution Press, Washington and London: 207-212.

Einsele G. 2000. — *Sedimentary Basins: Evolution, Facies, and Sediment Budget*. 2nd Edition. Springer, Berlin, 792 p.

Fields R. W. 1957. — Hystricomorph Rodents from the Late Miocene of Colombia, South America. *University of California Publications in Geological Sciences* 32 (5): 273-404.

Fields R. W. 1959. — Geology of the La Venta badlands, Colombia, South America. *University of California Publications in Geological Sciences* 32 (6): 405-444.

Flower B. P. & Kennett J. P. 1994. — The middle Miocene climatic transition: East Antarctic ice sheet development, deep ocean circulation and global carbon cycling. *Palaeogeography, Palaeoclimatology, Palaeoecology* 108: 537-555. https://doi.org/10.1016/0031-0182(94)90251-8

Flynn J. J., Guerrero J. & Swisher C. C. 1997. — Geochronology of the Honda Group, *in* Kay R. F., Madden R. H., Cifelli R. L. & Flynn J. J. (eds), *Vertebrate Paleontology in the Neotropics. The Miocene Fauna of La Venta, Colombia*. Smithsonian Institution Press, Washington and London: 44-59.

GEHRELS G., VALENCIA V. & PULLEN A. 2006. — Detrital Zircon Geochronology by Laser-Ablation Multicollector Icpms at the Arizona LaserChron Center. *The Paleontological Society Papers* 12: 67-76. https://doi.org/10.1017/S1089332600001352

GEHRELS G. E., VALENCIA V. A. & RUIZ J. 2008. — Enhanced precision, accuracy, efficiency, and spatial resolution of U-Pb ages by laser ablation – multicollector – inductively coupled plasma – mass spectrometry. *Geochemistry, Geophysics, Geosystems* 9 (3): 1-13. https://doi.org/10.1029/2007GC001805

GUERRERO J. 1993. — *Magnetostratigraphy of the Upper Part of the Honda Group and Neiva Formation. Miocene Uplift of the Colombian Andes*. PhD thesis, Duke University, Durham N. C., 108 p.

GUERRERO J. 1997. — Stratigraphy, sedimentary environments, and the Miocene uplift of the Colombian Andes, *in* KAY R. F., MADDEN R. H., CIFELLI R. L. & FLYNN J. J. (eds), *Vertebrate Paleontology in the Neotropics. The Miocene Fauna of La Venta, Colombia*. Smithsonian Institution Press, Washington and London: 15-43.

HAMON N., SEPULCHRE P., LEFEBVRE V. & RAMSTEIN G. 2013. — The role of eastern Tethys seaway closure in the middle Miocene Climatic Transition (ca. 14 Ma). *Climate of the Past* 9 (6): 2687-2702. https://doi.org/10.5194/cp-9-2687-2013

HECHT M. & LADUKE T. 1997. — Limbless Tetrapods, *in* KAY R. F., MADDEN R. H., CIFELLI R. L. & FLYNN J. J. (eds), *Vertebrate Paleontology in the Neotropics. The Miocene Fauna of La Venta, Colombia*. Smithsonian Institution Press, Washington and London: 95-99.

HERRIOTT T. M., CROWLEY J. L., SCHMITZ M. D., WARTES M. A. & GILLIS R. J. 2019. — Exploring the law of detrital zircon: La-Icp-Ms and Ca-Tims geochronology of Jurassic forearc strata, Cook Inlet, Alaska, USA. *Geology* 47 (11): 1044-1048. https://doi.org/10.1130/G46312.1

HETTNER A. 1892. — *Die Kordillere von Bogota*. Petermanns Geographische Mitteilungen, Ergänzungsheft, Heft, 104 p.

HILGEN F., LOURENS L. & VAN DAM J. A. 2012. — The Neogene Period, *in* GRADSTEIN F. M., OGG J. G., SCHMITZ M. & OGG G. (eds), *The Geologic Time Scale 2012*. Elsevier, Oxford: 923-978.

HOLBOURN A., KUHNT W., KOCHHANN K., ANDERSEN N. & MEIER S. 2015. — Global perturbation of the carbon cycle at the onset of the Miocene Climatic Optimum. *Geology* 43: 123-126. https://doi.org/10.1130/G36317.1

HORTON B. K. 2012. — Cenozoic evolution of hinterland basins in the Andes and Tibet, *in* BUSBY C. & AZOR A. (eds), *Tectonics of Sedimentary Basins: Recent Advances*. 1st edition. Blackwell Publishing Ltd., Oxford: 427-444.

HORTON B. K., PARRA M. & MORA A. 2020. — Construction of the Eastern Cordillera of Colombia: insights from the sedimentary record, *in* GÓMEZ J. & MATEUS-ZABALA D. (eds), *The Geology of Colombia*. Volume 3. *Paleogene – Neogene*. Servicio Geológico Colombiano, Bogotá: 67-88 (Publicaciones Geológicas Especiales; 37). https://doi.org/10.32685/pub.esp.37.2019.03

KAY R. F. & MADDEN R. H. 1997a. — Mammals and rainfall: paleoecology of the middle Miocene at La Venta (Colombia, South America). *Journal of Human Evolution* 32: 161-199. https://doi.org/10.1006/jhev.1996.0104

KAY R. F. & MADDEN R. H. 1997b. — Paleogeography and paleoecology, *in* KAY R. F., MADDEN R. H., CIFELLI R. L. & FLYNN J. J. (eds), *Vertebrate Paleontology in the Neotropics. The Miocene Fauna of La Venta, Colombia*. Smithsonian Institution Press, Washington and London: 520-550.

KELLY S. & OLSEN H. 1993. — Terminal fans – a review with reference to Devonian examples. *Sedimentary Geology* 85: 339-374. https://doi.org/10.1016/0037-0738(93)90092-j

KIDWELL S. M. & FLESSA K. W. 1996. — The Quality of the Fossil Record: Populations, Species, and Communities. *Annual Review of Earth and Planetary Sciences* 24 (1): 433-464. https://doi.org/10.1146/annurev.earth.24.1.433

LANGSTON W. & GASPARINI Z. 1997. — Crocodilians, Gryposuchus and the South American gavials, *in* KAY R. F., MADDEN R. H., CIFELLI R. L. & FLYNN J. J. (eds), *Vertebrate Paleontology in the Neotropics. The Miocene Fauna of La Venta, Colombia*. Smithsonian Institution Press, Washington and London: 113-154.

LUNDBERG J. G. 1997. — Freshwater fishes and their paleobiotic implications, *in* KAY R. F., MADDEN R. H., CIFELLI R. L. & FLYNN J. J. (eds), *Vertebrate Paleontology in the Neotropics. The Miocene Fauna of La Venta, Colombia*. Smithsonian Institution Press, Washington and London: 67-91.

LUDWIG K. R. (ed.) 2012. — *User's Manual for IsoPlot 3.75. A Geochronological Toolkit for Microsoft Excel*. Berkeley Geochronology Center, Berkeley, 75 p. (Special Publication; 5).

MADDEN R. H., GUERRERO J., KAY R. F., FLYNN J. J., SWISHER III, C. C. & WALTON A. H. 1997a. — The Laventan stage and age, *in* KAY R. F., MADDEN R. H., CIFELLI R. L. & FLYNN J. J. (eds), *Vertebrate Paleontology in the Neotropics. The Miocene Fauna of La Venta, Colombia*. Smithsonian Institution Press, Washington and London: 499-519.

MADDEN R. H., SAVAGE D. E. & FIELDS R. 1997b. — A History of Vertebrate Paleontology in The Magdalena Valley, *in* KAY R. F., MADDEN R. H., CIFELLI R. L. & FLYNN J. J. (eds), *Vertebrate Paleontology in the Neotropics. The Miocene Fauna of La Venta, Colombia*. Smithsonian Institution Press, Washington and London: 3-12.

MAKASKE B. 2001. — Anastomosing rivers: a review of their classification, origin and sedimentary products. *Earth-Science Reviews* 53: 149-196. https://doi.org/10.1016/S0012-8252(00)00038-6

MCDONALD H. G. 1997. — Xenarthrans: Pilosans, *in* KAY R. F., MADDEN R. H., CIFELLI R. L. & FLYNN J. J. (eds), *Vertebrate Paleontology in the Neotropics. The Miocene Fauna of La Venta, Colombia.* Smithsonian Institution Press, Washington and London: 233-245.

MIALL A. D. 1992. — Alluvial deposits, *in* WALKER R. G. & JAMES N. P. (eds), *Facies Models. Response to the Sea Level.* Geological Association of Canada Press, Ontario: 123-146.

MIALL A. D. 2006. — *The Geology of Fluvial Deposits. Sedimentary Facies, Basin Analysis, and Petroleoum Geology*. Springer, Berlin Heidelberg, 582 p.

MIDDLETON G. V. 1973. — Johannes Walther's Law of the correlation of facies. *Geological Society of America Bulletin* 84: 979-988. https://doi.org/10.1130/0016-7606(1973)84%3C979:JWLOTC%3E2.0.CO;2

MIDDLETON G. V. 2003. — *Encyclopedia of Sediments and Sedimentary Rocks*. Kluwer Academic Publishers, London, 805 p.

MONTES C., SILVA C. A., BAYONA G. A., VILLAMIL R., STILES E., RODRÍGUEZ-CORCHO A. F., BELTRÁN-TRIVIÑO A., LAMUS F., MUÑOZ-GRANADOS M. D., PÉREZ-ÁNGEL L. C., HOYOS N., GÓMEZ S., GALEANO J. J., ROMERO E., BAQUERO M., CÁRDENAS-ROZO A. L. & VON QUADT A. 2021. — A Middle to Late Miocene Trans-Andean Portal: Geologic Record in the Tatacoa Desert. *Frontiers in Earth Science* 8: 587022. https://doi.org/10.3389/feart.2020.587022

ORTIZ J. & JARAMILLO C. 2020. — SDAR: Stratigraphic Data Analysis. R package version 0.9-55. https://cran.r-project.org/

QGIS DEVELOPMENT TEAM. 2020. — QGIS Geographic Information System, version 3.10.2. Open Source Geospatial Foundation Project. http://qgis.osgeo.org

RAMÓN J. C. & ROSERO A. 2006. — Multiphase structural evolution of the western margin of the Girardot subbasin, Upper Magdalena Valley, Colombia. *Journal of South American Earth Sciences* 21 (4): 493-509. https://doi.org/10.1016/j.jsames.2006.07.012

REINECK H. & SINGH I. 1986. — *Depositional Sedimentary Environments. With Reference to Terrigenous Clasts*. 2nd edition. Springer-Verlag, Berlin Heidelberg New York, 551 p.

RODRÍGUEZ G., ARANGO M. I., ZAPATA G. & BERMÚDEZ J. G. 2018. — Petrotectonic characteristics, geochemistry, and U-Pb geochronology of Jurassic plutons in the Upper Magdalena Valley-Colombia: Implications on the evolution of magmatic arcs in the

Nw Andes. *Journal of South American Earth Sciences* 81: 10-30. https://doi.org/10.1016/j.jsames.2017.10.012

Royo Y Gómez J. 1941. — *Datos para la geología económica del Departamento del Huila*. Informe 312. Ministerio de Minas y Petróleos, Sección Técnica, Bogotá D.C., 102 p.

Royo Y Gómez J. 1942. — *Contribución al conocimiento de la geología del Valle Superior del Magdalena (Departamento del Huila).* Compilación de los estudios geológicos oficiales de Colombia, Servicio Geológico Nacional, Tomo V, Bogotá D.C.: 261-326.

Salazar-Jaramillo S., Sliwnski M. G., Hertwig A. T., Garzón C. C., Gómez C. F., Bonilla G. E. & Guerrero J. 2022. — Changes in rainfall seasonality inferred from weathering and pedogenic trends in mid-Miocene paleosols of La Tatacoa, Colombia. *Global and Planetary Change* 208: 1-17. https://doi.org/10.1016/j.gloplacha.2021.103711

Sarmiento L. F. & Rangel A. 2004. — Petroleum systems of the Upper Magdalena Valley, Colombia. *Marine and Petroleum Geology* 21 (3): 373-391. https://doi.org/10.1016/j.marpetgeo.2003.11.019

Sarmiento-Rojas L. F., Van Wess J. D. & Cloetingh S. 2006. — Mesozoic transtensional basin history of the Eastern Cordillera, Colombian Andes: Inferences from tectonic models. Journal of South American Earth Sciences 21 (4): 383-411. https://doi.org/10.1016/j.jsames.2006.07.003

Shaw A. B. 1964. — *Time in Stratigraphy*. McGraw Hill Book Co., New York, 365 p.

Stacey J. T. & Kramers J. D. 1975. — Approximation of terrestrial lead isotope evolution by a two-stage model. *Earth and Planetary Science Letters* 26 (2): 207-221. https://doi.org/10.1016/0012-821x(75)90088-6

Steinthorsdottir M., Coxall H. K., De Boer A. M., Huber M., Barbolini N., Bradshaw C. D., Burls N. J., Feakins S. J., Gasson E., Hendriks J., Holbourn A. E., Kiel S., Kohn M. J., Knoor G., Kürschner W. M., Lear C. H., Liebrand D., Lunt D. J., Mörs T., Pearson P. N., Pound M. J., Stoll H. & Strömberg C. A. E. 2021. — The Miocene: The future of the past. *Paleoceanography and Paleoclimatology* 36: e2020pa004037. https://doi.org/10.1029/2020pa004037.

Stirton R. A. 1953a. — A New Genus of Interatheres from the Miocene of Colombia. *University of California Publications In Geological Sciences* 29 (6): 265-348.

Stirton R. A. 1953b. — Vertebrate paleontology and continental stratigraphy in Colombia. *Bulletin of the Geological Society of America* 64: 603-622. https://doi.org/10.1130/0016-7606(1953)64[603:VPACSI]2.0.CO;2

Takai M., Takemura K., Takai A., Villarroel A. C., Hayashida A., Danhara T., Ohno T., Franco R., Setoguchi T. & Nogami Y. 1992. — Geology of La Venta, Colombia, South America. *Kyoto University Overseas Research Reports of New World Monkeys* 8: 1-17. http://hdl.handle.net/2433/199689

Takai M. & Setoguchi T. 1990. — Geology and Localities of Monkey Fossils in the La Venta Badlands, Colombia, South America. *Kyoto University Overseas Research Reports of New World Monkeys* 7: 1-7. http://hdl.handle.net/2433/199644

Takai M., Anaya F., Suzuki H., Shigehara N. & Setoguchi T. 2001. — A New Platyrrhine from the Middle Miocene of La Venta, Colombia and Phyletic Position of Callicebinae. *Anthropological Science* 109 (4): 289-307. https://doi.org/10.1537/ase.109.289

Takemura K. 1983. — Geology of the East Side Hills of the Rio Magdalena from Neiva to Villavieja, Colombia. *Kyoto University Overseas Research Reports of New World Monkeys* 3: 19-28. http://hdl.handle.net/2433/198713

Takemura K. & Danhara T. 1985. — Fission-Track Dating of the Upper Part of Miocene Honda Group in La Venta Badlands, Colombia. *Kyoto University Overseas Research Reports of New World Monkeys* 5: 31-38. http://hdl.handle.net/2433/199624

Takemura A., Takai M., Danhara T. & Setoguchi T. 1992. — Fission-track ages of the Villavieja Formation of the Miocene Honda Group in La Venta, Department of Huila, Colombia. *Kyoto University Overseas Research Reports of New World Monkeys* 8: 19-27. http://hdl.handle.net/2433/199688

Van Houten F. & Travis R. B. 1968. — Cenozoic Deposits, Upper Magdalena Valley, Colombia. *The American Association of Petroleum Geologist Bulletin* 52 (4): 675-702. https://doi.org/10.1306/5D25C455-16C1-11D7-8645000102C1865D

Valencia-Gómez J. C., Cardona A., Bayona G., Valencia V. & Zapata S. 2020. — Análisis de procedencia del registro sin-orogénico Maastrichtiano de la Formación Cimarrona, flanco occidental de la Cordillera Oriental colombiana. *Boletín de Geología* 42 (3): 171-204. https://doi.org/10.18273/revbol.v42n3-2020008

Villarroel C., Setoguchi T., Brieva J., & Macía C. 1996. — Geology of the La Tatacoa "Desert" (Huila, Colombia): Precisions on the Stratigraphy of the Honda Group, the Evolution of the "Pata High" and the Presence of the La Venta Fauna. *Memoirs of the Faculty of Science Kyoto University, Series of Geology and Mineralogy* 58 (1-2): 41-66. http://hdl.handle.net/2433/186679

Walton A. H. 1997. — Rodents, *in* Kay R. F., Madden R. H., Cifelli R. L. & Flynn J. J. (eds), *Vertebrate Paleontology in the Neotropics. The Miocene Fauna of La Venta, Colombia*. Smithsonian Institution Press, Washington and London: 392-409.

Watanabe T., Setoguchi T., & Shigehara N. 1979. — An outline of paleontological investigation. *Kyoto University Overseas Research Reports of New World Monkeys* 1: 39-45. http://hdl.handle.net/2433/198661

Wellman S. 1970. — Stratigraphy and Petrology of the Nonmarine Honda Group (Miocene), Upper Magdalena Valley, Colombia. *Geological Society of America Bulletin* 81: 2353-2374. https://doi.org/10.1130/0016-7606(1970)81[2353:SAPOTN]2.0.CO;2

You Y., Huber M., Muller R. D., Poulsen C. J. & Ribbe J. 2009. — Simulation of the middle Miocene Climate Optimum. *Geophysical Research Letters* 36: L04702. https://doi.org/10.1029/2008gl036571

Zachos J., Pagani M., Sloan L., Thomas E. & Billups K. 2001. — Trends, rhythms, and aberrations in global climate 65 Ma to Present. *Science* 292: 686-692. https://doi.org/10.1126/science.1059412

Zachos J., Dickens G. & Zeebe R. 2008. — An early Cenozoic perspective on greenhouse warming and carbon-cycle dynamics. *Nature* 451 (17): 279-283. https://doi.org/10.1038/nature06588

Zapata S., Cardona A., Jaramillo J. S., Patiño A., Valencia V., León S., Mejía D., Pardo-Trujillo A. & Castañeda J. P. 2019. — Cretaceous extensional and compressional tectonics in the Northwestern Andes, prior to the collision with the Caribbean oceanic plateau. *Gondwana Research* 66: 207-226. https://doi.org/10.1016/j.gr.2018.10.008

Submitted on 22 April 2022;
accepted on 12 September 2022;
published on 13 April 2023.

SUPPLEMENTARY MATERIEL/APPENDICES

Appendix 1. — Fossil reports from the La Venta site. Compilation from years 1929 to 2021. https://doi.org/10.5852/geodiversitas2023v45a6_s1

Appendix 2. — SDAR sections printed as PDFs and traverses. https://doi.org/10.5852/geodiversitas2023v45a6_s2

Appendix 3. — Excel formats for each section studied to place them into SDAR. https://doi.org/10.5852/geodiversitas2023v45a6_s3

Appendix 4. — R code to plot the stratigraphic sections in SDAR. https://doi.org/10.5852/geodiversitas2023v45a6_s4

Appendix 5. — QGIS project including all the geological cartography used in the ellaboration of this work with exception of Montes' *et al.* (2021) cartography which is available at: https://doi.org/10.3389/feart.2020.587022. https://doi.org/10.5852/geodiversitas2023v45a6_s5

Appendix 6. — Extended lithological resolution of the composite standard section of the Honda Group. Scale 1:1000. https://doi.org/10.5852/geodiversitas2023v45a6_s6

Appendix 7. — Extended lithofacies codes throughout the Honda Group. https://doi.org/10.5852/geodiversitas2023v45a6_s7

Appendix 8. — Geochronology dataset including frequency-distribution probability density plots: **A**, stratigraphic position of geochronological samples; **B**, geochronology samples; **C**, frequency-distribution Method raw-sample; **D**, frequency-distribution Probability-density raw-sample; **E**, probability-density Method raw-sample; **F**, frequency-distribution Probability-density Processed-sample; **G**, frequency-distribution Probability-density Processed-sample; **H**, probability-density Method Processed-sample; **I**, frequency-distribution new samples U-Pb; **J**, probability-density new samples U-Pb. https://doi.org/10.5852/geodiversitas2023v45a6_s8

Appendix 9. — Extended methodology of the Age Model. https://doi.org/10.5852/geodiversitas2023v45a6_s9

Appendix 10. — Detailed information about the stratigraphic and geographic position of each fossil locality. https://doi.org/10.5852/geodiversitas2023v45a6_s10

Appendix 11. — Graphic correlations: **A**, this work vs Fields (1959; sections B-C); **B**, this work vs Fields (1959; sections D-E); **C**, this work vs Fields (1959; sections F-J); **D**, this work vs Guerrero (1997; sections A-G); **E**, this work vs Guerrero (1997; sections B-C); **F**, this work vs Guerrero (1997; sections D-F); **G**, this work vs Takai *et al.* (2001; sections a-b); **H**, this work vs Zurita *et al.* (2013); **I**, relation between Montes' *et al.* (2021) cartographic units and the composite section. https://doi.org/10.5852/geodiversitas2023v45a6_s11

Appendix 12. — Additional stratigraphic sections this work. https://doi.org/10.5852/geodiversitas2023v45a6_s12

Appendix 13. — Reported fauna from the La Victoria Formation. https://doi.org/10.5852/geodiversitas2023v45a6_s13

Appendix 14. — Reported fauna from the Villavieja Formation. https://doi.org/10.5852/geodiversitas2023v45a6_s14

Appendix 15. — New magnetostratigraphic interpretation compared to the interpretation by Flynn *et al.* (1997). https://doi.org/10.5852/geodiversitas2023v45a6_s15

Appendix 16. — Cluster between fossil localities and lithofacies associations. https://doi.org/10.5852/geodiversitas2023v45a6_s16